공학박사 학위논문

Evaluation of material yield property using spherical indentation and surface displacement analysis

2020 년 8 월

서울대학교 대학원

재료공학부

권 오 민

Evaluation of material yield property using spherical indentation and surface displacement analysis

압입시험 및 표면 변위 분석을 이용한 재료의 항복 특성 평가

지도 교수: 권 동 일

이 논문을 공학박사 학위논문으로 제출함

2020 년 7 월

서울대학교 대학원

재료공학부

권 오 민

권오민의 공학박사 학위논문을 인준함

2020 년 7 월

위 원 장	박 은 수	(인)
부위원장	권 동 일	(인)
위 원	최 인 석	(인)
위 원	전 은 채	(인)
위 원	권 혁 선	(인)

Evaluation of material yield property using spherical indentation and surface displacement analysis

A DISSERTATION SUBMITTED TO
DEPARTMENT OF MATERIALS SCIENCE AND ENGINEERING
SEOUL NATIONAL UNIVERSITY

FOR THE DEGREE OF
DOCTOR OF PHILOSOPHY

OH MIN KWON

August 2020

Abstract

Kwon, Oh Min
Dept. Materials Science and Engineering
The Graduate School
Seoul National University

Assessment of reliability for structural materials requires various information such as operating conditions, applied stresses, defect characteristics, mechanical properties, etc. The operating conditions and applied stress can be estimated by the design stress, and defect characteristics can be measured by nondestructive tests such as acoustic emission and ultrasonic test. However, it is difficult to evaluate the mechanical properties in the field using the conventional mechanical tests. Mechanical properties are basic data to analyze the reliability of the structure, and are measured with a sample specified in international standards. Since international standard tests require sample with specific shapes and sizes, it is impossible to evaluate the mechanical properties of structures in the field, and it is difficult to apply them to materials with small scales and complex shapes. Therefore, a nondestructive way to measure in-service material properties is highly desirable to assess the reliability of structural materials.

Instrumented indentation testing (IIT), developed from conventional hardness testing, provides not only hardness and elastic modulus but also high-level information such as tensile properties, residual stress and fracture toughness through elasto plastic analysis of the continuously measured load and depth curves. In addition, it can be used at various scales from micro-scale to nano-scale by controlling the size of the indenter and the load or depth range. Therefore, many studies have been conducted for decades now on IIT to evaluate mechanical properties as well as hardness and elastic modulus. Especially, the yield strength among the mechanical properties is defined as the limit stress at which permanent deformation occurs, so yield strength is one of the most important parameters used in reliability assessment to predict material plastic deformation and fracture.

Previous studies have suggested experimental or analytical relationships between yield strength and spherical indentation parameters, and were successfully verified for material with various strain-hardening behaviors. However, the indentation yield strength models proposed in the previous studies have some limitations. First, since directionality was not considered in many spherical indentation models, there is a limitation that it cannot be applied to materials with anisotropy such as rolled material, extruded material and 3D printing material, etc. Seconds, research on the uncertainty in yield strength is needed because the stress variation at the yield point is more severe than at the necking point, increasing the standard uncertainty.

Moreover, so far the uncertainty different in the yield strength as measured by the spherical indentation and uniaxial tensile testing remains unclear and it is still unknown how uncertainty sources quantitatively affect the uncertainty of indentation yield strength.

In this study, in terms of applying the spherical indentation to more diverse materials, we attempted to derive an indentation yield strength model considering directionality using dimensional analysis of single spherical indentation. In order to obtain the basic data of the modeling, FEA simulation was performed on various imaginary materials which were made by giving different yield strength, direction ratio of yield strength and strain-hardening exponent. Applying the Π-theorem in dimensional analysis, we obtained a model of indentation yield strength considering directionality. Subsequently, we analyzed the displacement distribution around the impression for all imaginary materials, from which a phenomenological model was derived to evaluate the direction ratio of yield strength. The model proposed in this study was verified through surface displacement analysis of metallic materials with Digital Image Correlation (DIC). In addition, in terms of the effect of the data deviation of spherical indentation, we proposed a method for accurately evaluating the uncertainty of indentation yield strength calculated from the modified Meyer relation as a mathematical function of the measurement, taking into account Type A and Type B uncertainty. Using this method, we investigated the effect of the

major sources of uncertainty in the indentation system to interpret the difference in uncertainty between indentation and uniaxial tensile testing. Finally, acceptable uncertainty sources are proposed that give the indentation similar uncertainty to uniaxial tensile testing.

Keyword: Indentation; Spherical indenter; Yield strength; Anisotropy; Directionality; Indentation surface displacement; Digital image correlation; Uncertainty

Student Number: 2013-23033

Table of Contents

LIST OF TABLES

Chapter 2

Chapter 3

Chapter 4

Table 4.3. Degree of contribution of measurands on expanded uncertainty of indentation yield strength

LIST OF FIGURES

Chapter 2

Chapter 3

Chapter 4

Chapter 1

INTRODUCTION

Contents

1.1. Objective of the Thesis

Many structural materials are subjected to forces or loads when in service, which can lead to plastic deformation and severe damage, so it is essential to analyze safety and reliability of structural materials. One of the most important mechanical properties for safety and reliability assessment is yield strength, which is defined as the limit stress at which permanent deformation occurs. The yield strength is determined from the stress and strain curve obtained by the uniaxial tensile test based on the international standard [1]. Standard test method generally requires specific specimen geometry and size. Moreover, because the testing procedures are relatively complex, it must be well controlled to obtain valid data. These limitations make it possible to evaluate the yield strength of structures in the field, and it is difficult to apply them to materials with small scales and complex shapes.

Because instrumented indentation testing (IIT), developed from conventional hardness testing, provides not only hardness and elastic modulus but also high-level information such as tensile properties, residual stress and fracture toughness through elasto-plastic analysis of

the continuously measured load and depth curves. Since the testing procedure of IIT is simple and easy, it is widely used at scales ranging from the large-scale testing for power plants, pipelines and vessels to small-scale testing of thin film samples, MEMS, and bio-materials [2, 3]. However, hardness cannot be directly correlated with the yield strength obtained by uniaxial tensile testing, even though it is generally considered to be resistance to plastic deformation. Many researches [4-6] have been conducted to find the physical meaning of hardness and derive a relationship between yield strength and hardness.

Tabor [7] proposed a direct relationship between flow stress and strain in uniaxial tension and such spherical indentation parameters as indentation load, contact radius and indenter radius. However, Tabor's approach is only valid in the limit of fully developed plasticity and the relationship is between flow stress and hardness, not the yield strength. Since Tabor's work, expanding cavity models (ECMs) have been developed to describe the indentation response of various materials. Johnson [8] analyzed the transition region between perfectly elastic and fully developed plasticity beneath the indenter, and developed an ECM by adapting Hill's cavity model [9] with a hydrostatic hemispherical core beneath the spherical indenter. Jonson's ECM explains how the ratio of

hardness to yield stress varies with the ratio of elastic modulus to yield strength and the angle of inclination of the conical indenter to the surface at the edge of the indentation. Following Jonson's results, attempts have been made to modify the ECM for strain-hardening materials. Studman et al. [10] suggested a modification that considers variations in the hydrostatic uniform pressure in the core as values that obey the von Mises yield criterion. Recently, Kang et al. [11] modified the relationship between yield strength and Brinell hardness (the so-called Meyer relation [6]) using the results of stress-filed analysis and constitutive equation. And, the indentation yield strength from the Kang et al.'s model showed good agreement with the yield strength measured by uniaxial tensile testing for metallic materials with various strain-hardening behaviors.

In addition to the analytical approach, many studies [3, 12-14] have been attempted to use dimensional analysis to relate indentation parameters to mechanical response. Dimensional analysis is a mathematical technique to reduce the number of related variables in order to more easily confirm or describe the correlation between the independent and dependent variables related to physical laws. Therefore, dimensional analysis is widely used to define scaling variables and universal functions. Finite element simulations and dimensional analyses

have been used in several studies [13] to characterize frictional sliding in elasto-plastic materials, and it was found that a scratch hardness extracted from frictional sliding experiments can be correlate with the yield strength. In addition, methods have been proposed to evaluate the anisotropic plastic properties of materials using dimensional analysis of spherical indentation. A. Yonezu et al. [15, 16] improved the single spherical indentation method to evaluate anisotropic plastic properties by employing dimensional analysis and the representative strain concept for the material with plasticity governed by Hill's yield criterion. They established the dimensionless function including the anisotropic plastic properties and pile-up height around the impression by performing extensive finite element simulation. They proposed that the pile-up height in the transverse direction becomes higher than that in the longitudinal one for the SiC whisker-reinforced aluminum alloy. That is, the plastic properties with different among orthogonal directions can be estimated by using this characteristics and the indentation load and depth curve. However, since plastic deformation around impressions such as plastic pile-up or sink-in height can be measured with very precise experimental equipment, it is difficult to obtain valid data and cannot be evaluated in

the field. Therefore, research is needed to more easily and efficiently evaluate the plastic anisotropic properties of materials.

As mentioned above, new researches are actively underway that combine finite element simulation and dimensional analysis with IIT, but little work has been done on the validity of measurement data. Since the data by repeated experiments show scattering characteristics, the true value cannot be defined, so the concept of uncertainty is necessary to confirm the validity of the experiment data. According to ISO GUM [17], uncertainty is a parameter describing doubt about the validity of a measurement result and characterizes the dispersion of a value that could reasonably be attributed to the measurand. Research on the uncertainty in yield strength in particular is needed because the stress variation at the yield point is more severe than at the necking point, increasing the standard uncertainty. Jeon et al. [18] suggested a simplified uncertainty estimation method for indentation yield strength and tensile strength through measurands defined by a mathematical model. However, they did not take into account all types of uncertainty, and whether the uncertainty depends on indentation yield strength was not confirmed for metallic materials with various hardening behaviors. Therefore, research is needed

to accurately evaluate the uncertainty of data or results obtained by indentation testing based on international standards.

This study focused on the yield strength, which is the most important for the reliability analysis of structures among various mechanical properties, and tried to develop a model which can evaluate the yield strength with different among orthogonal directions. In the first part of this study, we attempted to derive an evaluation model of indentation yield strength considering directionality induced by plastic deformation. In order to obtain basic data of modeling, finite element simulation was conducted, and imaginary materials were made by changing yield strength, directional ratio of yield strength and strain-hardening exponent. Spherical indentation tests were performed on these imaginary materials, and a model was established based on Buckingham′s PI-theorem, one of the dimensional analyzes, using the data set related to the indentation response. For verification of the model established by dimensional analysis, we confirmed the relative error between the input yield strength of x-axis and the yield strength of x-axis calculated from the model. In order to determine the direction ratio of yield strength included the model, a surface displacement distribution around the impression was analyzed

based on the finite element simulation. The displacement change in the x- and y-axis around the impression was analyzed depending on various direction ratio of yield strength, and it was confirmed how the relationship between the direction ratio of yield strength and that of the displacement was affected by tensile properties. For the results obtained by simulation data, experimental verification was performed with Digital Image Correlation (DIC) method which can obtain mechanical response by image analysis. In the second part of this study, we used the modified Meyer relation [11] recently developed by stress field analysis to evaluate the uncertainty of yield strength calculated by the indentation testing. Based on the international standards [17, 19, 20], a relationship between the uncertainty and the indentation yield strength was demonstrated for metallic materials with various strain-hardening behaviors. Using the method proposed in this study, we quantitatively the uncertainty level of the yield strength as estimated by the indentation testing and uniaxial tensile testing. To determine the dominant measurand related to indentation load and depth data, the degree of contribution and the coefficient of variation of each measurand were analyzed. Based on these results, we verified the effects of two possible uncertainty sources influenced by surface contact: indentation sample surface roughness and

angular misalignment between the surface normal of the sample and the symmetric axis of the spherical indenter. From the relationship between the uncertainty and the possible uncertainty sources, we proposed acceptable surface roughness and standard uncertainty of the angular misalignment.

1.2. Organization of the Thesis

This thesis has four parts. After a brief introduction in Chapter 1, Chapter 2 gives a historical overview of hardness measurement by the spherical indenter. Chapter 2 also gives a detailed description of indentation stress fields for both elastic and elastic-plastic contact, from which is derived the basic principle of the instrumented indentation tests (IIT), a nondestructive technique for evaluating mechanical properties such as hardness, elastic modulus, tensile properties, residual stress, fracture toughness, and the like. Theoretical models for estimating yield property of anisotropic materials are presented in Chapter 3. From the dimensional analysis, the indentation yield strength model considering directionality is newly proposed and model of direction ratio of yield strength is developed based on the analysis of surface displacement distribution. In Chapter 4, issues of field application of the IIT are discussed, and the uncertainty evaluation method and standards of indentation yield strength are discussed in terms of uncertainty.

References

[1] A. E8/E8M-16a, *Standard Test Method for Tension Testing of Metallic Materials*, ASTM International (2016).

[2] W.C. Oliver, G.M. Pharr, An improved technique for determining hardness and elastic modulus using load and displacement sensing indentation experiments, Journal of materials research 7(6) (1992) 1564-1583.

[3] Y.-T. Cheng, C.-M. Cheng, Scaling, dimensional analysis, and indentation measurements, Materials Science and Engineering: R: Reports 44(4) (2004) 91-149.

[4] R. A. George, S. Dinda, A. S. Kasper, Estimating yield strength from hardness data, 1976.

[5] F.M. Haggag, R.K. Nanstad, J.T. Hutton, D.L. Thomas, R.L. Swain, Use of automated ball indentation testing to measure flow properties and estimate fracture toughness in metallic materials, Applications of automation technology to fatigue and fracture testing, ASTM International1990.

[6] E. Meyer, Investigations of hardness testing and hardness, Phy. Z. 9

(1908) 66-74.

[7] D. Tabor, The hardness of metals, Clarendon, Oxford, 1951.

[8] K.L. Johnson, The correlation of indentation experiments, Journal of the Mechanics and Physics of Solids 18(2) (1970) 115-126.

[9] R. Hill, The mathematical theory of plasticity, Clarendon, Oxford 613 (1950) 614.

[10] C.J. Studman, M.A. Moore, S.E. Jones, On the correlation of indentation experiments, Journal of Physics D: Applied Physics 10(6) (1977) 949-956.

[11] S.-K. Kang, Y.-C. Kim, K.-H. Kim, J.-Y. Kim, D. Kwon, Extended expanding cavity model for measurement of flow properties using instrumented spherical indentation, International Journal of Plasticity 49 (2013) 1-15.

[12] S. Suresh, T.-G. Nieh, B. Choi, Nano-indentation of copper thin films on silicon substrates, Scripta Materialia 41(9) (1999) 951-957.

[13] M. Dao, N.v. Chollacoop, K. Van Vliet, T. Venkatesh, S. Suresh, Computational modeling of the forward and reverse problems in instrumented sharp indentation, Acta materialia 49(19) (2001) 3899-3918.

[14] S. Bellemare, M. Dao, S. Suresh, The frictional sliding response of elasto-plastic materials in contact with a conical indenter, International

Journal of Solids and Structures 44(6) (2007) 1970-1989.

[15] A. Yonezu, Y. Kuwahara, K. Yoneda, H. Hirakata, K. Minoshima, Estimation of the anisotropic plastic property using single spherical indentation—An FEM study, Computational Materials Science 47(2) (2009) 611-619.

[16] A. Yonezu, K. Yoneda, H. Hirakata, M. Sakihara, K. Minoshima, A simple method to evaluate anisotropic plastic properties based on dimensionless function of single spherical indentation – Application to SiC whisker-reinforced aluminum alloy, Materials Science and Engineering: A 527(29) (2010) 7646-7657.

[17] ISO, Uncertainty of measurement - Part 3 : Guide to the expression of uncertainty in measurement(GUM:1995), ISO/IEC GUIDE 98-1:2009(E) (**2008**).

[18] E.-c. Jeon, J.-S. Park, D.-S. Choi, K.-H. Kim, D. Kwon, A Method for Estimating Uncertainty of Indentation Tensile Properties in Instrumented Indentation Test, 2009.

[19] E.c.-o.f. Accreditation, EA Guidelines on the estimation of uncertainty in hardness measurements, (2002).

[20] EURAMET, Guidelines on the Estimation of Uncertainty in Hardness Measurements, (2007).

Chapter 2

RESEARCH BACKGROUND

Contents

2.1. Contact Mechanics

2.1.1. Elastic Contact

Hertz [1, 2] first studied localized deformation and pressure distribution for two elastic bodies contact based on elastic contact mechanics. The assumption of Hertz theory can be summarized as follows:

(1) The surfaces of the material are continuous and non-conforming.

(2) The materials have small strains due to only elastic deformation.

(3) Each solid is considered as an elastic half-space.

(4) The surfaces have no friction.

Hertz suggested that the ellipsoid pressure distribution satisfies the boundary condition of the problem and analyzed the normal pressure beneath a spherical indenter for the case of a sphere.

$$\frac{\sigma_z}{p_m} = -\frac{1}{2}\left(1-\frac{r^2}{a^2}\right)^{-1/2} \tag{2-1}$$

where the mean contact pressure (P_m) is calculated from the indentation load divided by projected contact area and a is the contact radius of spherical impression.

For the pressure distribution obtained by Eq. (2-1), the relationship between the normal stress and mean pressure ($\sigma_z = 1.5 \cdot P_m$) is maximized at the center of contact surface and is zero at the edge of the contact surface. Outside the contact surface, σ_z becomes zero along the surface. The displacement distribution within the contact circle is:

$$u_z = \frac{1-\upsilon^2}{E}\frac{3}{2}P_m\frac{\pi}{4a}\left(2a^2 - r^2\right) \tag{2-2}$$

where E is elastic modulus, υ is Poisson's ratio and r is radial displacement. And, the displacement distribution outside of the contact circle can be expressed as:

$$u_z = \frac{1-\upsilon^2}{E}\frac{3}{2}P_m\frac{1}{2a}\left[\left(2a^2 - r^2\right)\sin^{-1}\frac{a}{r} + r^2\frac{a}{r}\left(1-\frac{a^2}{r^2}\right)^{1/2}\right] \tag{2-3}$$

Eq. (2-2) and Eq. (2-3) give displacements of points on the material surface subjected to the pressure distribution obtained by Eq. (2-1). For a perfectly rigid indenter, Eq. (2-1) at $r = 0$ gives the penetration depth beneath the original surface and also the distance of mutual approach between two displacement points in both the indenter and material. Eq. (2-2) shows that the depth beneath the original surface of the contact circle is exactly one-half the total depth at $r = 0$.

The displacement distribution of points on the surface beneath the indenter in the radial direction is expressed by:

$$u_z = \frac{(1-2\upsilon)(1+\upsilon)}{3E}\frac{a^2}{r}\frac{3}{2}P_m\left[1-\left(1-\frac{r^2}{a^2}\right)^{3/2}\right] \tag{2-4}$$

The radial displacement distribution outside the contact circle is expressed by:

$$u_z = \frac{(1-2\upsilon)(1+\upsilon)}{3E}\frac{a^2}{r}\frac{3}{2}P_m \tag{2-5}$$

Using the cylindrical coordinate system, the ratios of stresses to mean

contact pressure in the contact circle in the surface can be expressed by:

$$\frac{\overline{\sigma_{rr}}}{P_m} = \frac{1-2\upsilon}{2}\left(\frac{a^2}{r^2}\right)\left[1-\left(1-\frac{r^2}{a^2}\right)^{3/2}\right]-\frac{3}{2}\left(1-\frac{r^2}{a^2}\right)^{1/2} \tag{2-6}$$

$$\frac{\overline{\sigma_{\theta\theta}}}{P_m} = -\frac{1-2\upsilon}{2}\left(\frac{a^2}{r^2}\right)\left[1-\left(1-\frac{r^2}{a^2}\right)^{3/2}\right]-3\upsilon\left(1-\frac{r^2}{a^2}\right)^{1/2} \tag{2-7}$$

$$\frac{\overline{\sigma_{zz}}}{P_m} = -\frac{3}{2}\left(1-\frac{r^2}{a^2}\right)^{1/2} \tag{2-8}$$

And the ratio of radial stress to mean contact pressure outside the contact circle is expressed by:

$$\frac{\overline{\sigma_{rr}}}{P_m} = -\frac{\overline{\sigma_{\theta\theta}}}{P_m} = -\frac{(1-2\upsilon)}{2}\frac{a^2}{r^2} \tag{2-9}$$

All compressive stresses have maximum value as $(1-2\upsilon)P_0/3$ except at the very edge of contact where the radial stress is tensile.

Therefore, it is held responsible for the ring cracks in indentation mainly observed in brittle materials such as glass. The ratios of stresses to mean contact pressure beneath the surface along the z-axis are given as follows:

$$\frac{\sigma_{rr}}{P_m} = \frac{\sigma_{\theta\theta}}{P_m} = -\frac{3(1+\upsilon)}{2}\left[1 - \frac{z}{a}\tan^{-1}\left(\frac{a}{z}\right)\right] + \frac{3}{4}\left(1+\frac{z^2}{a^2}\right)^{-1} \tag{2-10}$$

$$\frac{\sigma_{zz}}{P_m} = -\frac{3}{2}\left(1+\frac{z^2}{a^2}\right)^{-1} \tag{2-11}$$

The principal shear stress has a value of about $0.31 \cdot P_0$ at a depth of $0.48 \cdot a$ for materials with $\upsilon = 0.3$. This is the maximum shear stress exceeding the shear stress at the origin ($0.10 \cdot P_0$), and also the shear stress in the surface at the edge of the contact ($0.13 \cdot P_0$). Therefore, plastic yielding would be expected to begin beneath the surface.

The mean pressures in an elastic semi-infinite solid indented by a rigid wedge, cone, cylinder and sphere are summarized in Table 2.1. The theoretical infinite pressure occurring at the apex of a wedge or cone calls for comment. The stress system at this apex is virtually hydrostatic, and it

would be exactly so for a incompressible material ($\upsilon = 0.5$). This means that the extent of plastic flow induced by the high pressure at the apex is very small and included within a small region very close to the apex. Significant plastic deformation begins only when the mean pressure exceeds $0.91 \cdot \sigma_y$ for the wedge and $0.50 \cdot \sigma_y$ for the cone. Nevertheless, as in cylindrical and spherical indenters, the plastic region is confined to a small region beneath the indenter. Therefore, it is fairly gradual that the departure of the mean pressure from its elastic value in the early stage of plastic deformation. For this reason, Hertz's original proposal that the first yield point could be used as a rational measure of hardness proved to be impractical.

2.1.2. Elastic-Plastic Contact

An indentation initially induces elastic deformation, due to the finite radius of the indenter tip, but it very quickly induces plastic deformation in the material with increasing indentation load. When the yield point is first exceeded the plastically deformed zone is small and fully contained by elastically deformed zone, so that the plastic strains have the same order of magnitude with the surrounding elastic strains. In this situation, the material displaced by the indenter is accommodated by an elastic expansion of the surrounding material. As the indentation becomes more severe by increasing the load on the indenter, increasing pressure is required beneath the indenter to produce the necessary expansion. Finally, the plastic zone comes out to the free surface and the displaced material is free to escape by plastic flow to the sides of the indenter.

It is difficult to find a theoretical solution of the elasto-plastic indentation stress-field due to the complexity of plastic deformation within the material. Since plastic strains in indentation are very much larger than any of the elastic strains, the sample is usually held to behave as a rigid-plastic material in which plastic flow is assumed to be governed by flow velocity considerations.

2.1.2.1. Slip-line field theory

In the slip-line field solution, developed originally in two dimensions by Hill and Lee, [3, 4], the volume of material displaced by the indenter is accounted for by upward flow, as shown in Fig. 2.1. The material in the region ABCDE flows upward and outward as the indenter moves downward under load. Because frictionless contact is assumed, the direction of stress along the line AB is normal to the face of the indenter. The lines within the region ABDEC are oriented at 45° to AB and are called slip lines (lines of maximum shear stress). This type of indentation involves a cutting of the sample material along the line OA and the creation of new surfaces that travel upward along the contact surface. The contact pressure across the face of the indenter is given by

$$P_m = 2\tau_{\max}(1+\alpha) = H \tag{2-12}$$

where $\tau_{\max}$ is the maximum value of shear stress in the sample material and α is the cone semi-angle (in radians). Invoking the Tresca shear stress criterion, where plastic flow occurs at $\tau_{\max} = 0.5\sigma_y$, and substituting into

Eq. (2-12) gives

$$H = \sigma_y(1+\alpha), \text{ where } \psi = 1+\alpha \qquad (2\text{-}13)$$

The constraint factor determined by this method is referred to as ψ_{flow}. For values of between 70° and 90°, Eq. (2-13) gives only a small variation in ψ_{flow} of 2.2 to 2.6. Friction between the indenter and the sample increases the value of ψ_{flow}. A slightly larger value for ψ_{flow} is found when the von Mises stress criterion is used (where $\tau_{\max} = 0.58\sigma_y$). For example, at α = 90°, Eq. (2-13) with the von Mises criterion gives $\psi = 3$.

2.1.2.2. Expanding cavity model

An alternative approach to the analysis of an elastic-plastic indentation follows an early suggestion of Bishop, Hill & Mott (1945) [3], as developed by Marsh (1964) [5] and Johnson (1970) [6]. It is based on the observations of Samuels & Mulhearn (1956) and Mulhearn (1959) [7]

that the sub-surface displacements produced by any blunt indenter are approximately radial from the point of first contact, with roughly hemispherical contours of equal strain.

In this simplified model of an elastic-plastic indentation, Johnson thought of the contact surface of the indenter as being encased in a hemispherical core of radius (a) as shown in Fig. 2.2. Within the core, there is assumed to be a hydrostatic component of stress $\bar{p}$. Outside the core, it is assumed that the stresses and displacements have radial symmetry and are the same as in an infinite elastic and perfectly plastic body containing a spherical cavity under a pressure $\bar{p}$. The elastic-plastic boundary lies at a radius c, where $c > a$. At the interface between core and the plastic zone, (a) the hydrostatic stress in the core is just equal to the radial component of stress in the external zone, and (b) the radial displacement of particles lying on the boundary $r = a$ during an increment of penetration dh must accommodate the volume of material displaced by the indenter (neglecting compressibility of the core).

The stresses in the plastic zone, $a \le r \le c$, are given by:

$$\frac{\sigma_{rr}}{\sigma_y} = -2\ln(c/r) - 2/3 \tag{2-14}$$

$$\frac{\sigma_{\theta\theta}}{\sigma_y} = -2\ln(c/r) + 1/3 \tag{2-15}$$

In the elastic zone, $r \ge c$:

$$\frac{\sigma_{rr}}{\sigma_y} = -\frac{2}{3}(c/r)^3 \tag{2-16}$$

$$\frac{\sigma_{\theta\theta}}{\sigma_y} = \frac{1}{3}(c/r)^3 \tag{2-17}$$

At the boundary of the core, the core pressure is given by

$$\frac{\bar{p}}{\sigma_y} = -\left[\frac{\sigma_{rr}}{\sigma_y}\right]_{r=a} = 2/3 + 2\ln(c/a) \tag{2-18}$$

The radial displacements are given by:

$$\frac{du_r}{dc} = \frac{\sigma_y}{E}\left\{3(1-\nu)(c^2/r^2) - 2(1-2\nu)(r/c)\right\} \tag{2-19}$$

Conservation of volume of the core requires:

$$2\pi a^2 du_r\Big|_{r=a} = \pi a^2 dh = \pi a^2 \tan\beta \, da \tag{2-20}$$

where β is the inclination of the face of the cone to the surface. If we set $r = a$ in Eq. (2-19) and note that for a conical indenter the geometrical similarity of the strain field with continued penetration requires that $dc/da = c/a$ = constant, then Eqs. (2-19) and (2-20) locate the elastic-plastic boundary by:

$$E\tan\beta/\sigma_y = 6(1-\nu)(c/a)^3 - 4(1-2\nu) \tag{2-20}$$

Substitution for (c/a) in Eq. (2-18) gives the pressure in the core. For an incompressible material a simple expression is obtained:

$$\frac{\bar{p}}{\sigma_y} = \frac{2}{3}\left\{1 + \ln\left(\frac{1}{3}\frac{E\tan\beta}{\sigma_y}\right)\right\} \tag{2-21}$$

Of course, the stress in the material immediately below an indenter is not purely hydrostatic. If $\bar{p}$ denotes the hydrostatic component, the normal stress will have a value $\sigma_{zz} \approx -(\bar{p} + 2\sigma_y/3)$ and the radial stress $\sigma_{rr} \approx -(\bar{p} - \sigma_y/3)$. A best estimate of the indentation pressure for the spherical cavity model would therefore be $\bar{p} + 2\sigma_y/3$. It appears from Eq. (2-21) that the pressure in the hydrostatic core beneath the indenter is a function of the single dimensionless variable $E\tan\beta/\sigma_y$, which may be interpreted as the ratio of the strain imposed by the indenter ($\tan\beta$) to the elastic strain capacity of the material (σ_y/E). Elasticity of the indenter can be taken into account by replacing E by reduced modulus E_r.

2.2. Instrumented Indentation Technique

2.2.1. Introduction to Instrumented Indentation Technique (IIT)

Instrumented indentation testing (IIT), developed from conventional hardness testing, can evaluate hardness and elastic modulus without optical measurement through elasto-plastic analysis of the continuously measured load and depth curves [8]. In addition, it can be used at various scales from micro-scale to nano-scale by controlling the size of the indenter and the load or depth range A macro-indentation used mainly in the safety assessment of an in-service component due to its nondestructive feature. Micro and nano-indenatation is now one of the most powerful tools for evaluating material properties and deformation behavior at small scales as thin films, MEMS, and bio-tissues [8, 9].

Over the past decade, the standardizations with regard to instrumented indentation test have become active discussion all over the world. The ISO 14577-1 as the most fundamental standard specifies not only the method of instrumented indentation test for hardness and material parameter, but the method of verification and calibration of testing machine. The part of ISO 14577-4 which describes a method for

testing coatings that is particularly suitable for testing in the micro/nano range is also under discussion. In addition, a new ISO technical report, ISO/TR 29381, has been established that describes three methods by which instrumented indentation tests can determine the tensile properties and residual stress of metallic materials.

2.2.2. Basic properties

The instrumented indentation test has been widely used to extract elastic modulus and hardness of the sample material from experimental indentation load and depth [8]. When load is removed from the indenter, the material attempts to regain its original shape, but it prevented from doing so because of plastic deformation. However, there is some degree of recovery due to the relaxation of elastic strains within the material. An analysis of the initial portion of this elastic unloading response gives an estimate of the elastic modulus of the indented material. A schematic draw of an indentation load and depth curve obtained with a spherical indenter is illustrated in Fig. 2.3. There are three important quantities that must be measured from the load and depth curves: the maximum load (L_{max}), the maximum displacement (h_{max}) and the elastic unloading

stiffness (S), defined as the slope of the upper portion of the unloading curve during the initial stages of unloading (also called the contact stiffness). The accuracy of hardness and modulus measurement depends inherently on how well these parameters can be measured experimentally. Another important quantity is the final depth (h_f) the permanent depth of penetration after the indenter is fully unloaded.

The form of the unloading curves for the most common types of indenter usually well approximated by the power law relation

$$L = a(h - h_f)^b \tag{2-22}$$

where a and b are power law fitting constants [1, 2, 8]. In the flat punch, the contact area remains constant as the indenter is removed, and resulting unloading curve is linear (b = 1). In the sharp and spherical indenters, experiments have shown that unloading curves are distinctly curved (b > 1). From the Eq. (2-22), the contact stiffness can be obtained as below:

$$S = \left.\frac{dL}{dh}\right|_{h=h_{\max}} = a \cdot b \cdot (h_{\max} - h_f)^{b-1} \tag{2-23}$$

Determination of the precise contact depth is the most important step in evaluating elastic modulus and hardness, since those are strongly dependent on it. During spherical indentation, materials show two types of responses: elastic deflection and plastic pile-up or sink-in. Using contact mechanics, Oliver and Pharr [8] expressed elastic deflection (h_d) as:

$$h_d = w\frac{L_{\max}}{S} \tag{2-24}$$

where w is a constant that depends on the geometry of the indenter. Important values are: w = 0.72 for a conical punch, w = 0.75 for a parabolic of revolution (which approximates to a sphere at small depths), and w = 1.00 for a flat punch [1, 2, 8]. The other response to spherical indentation is plastic pile-up/sink-in behavior [10, 11], which has been found to depend on the work-hardening exponent (n) and h_{max}/R.

$$h_{pile} = f\left(n, \frac{h_{\max}}{R}\right) \tag{2-25}$$

where h_{pile} is plastic pile-up height and h_c is contact depth. Using Eq. (2-25) to approximate the vertical displacement of the contact periphery, it follows from the geometry that the depth along which contact (h_c) is made between the indenter and the sample as shown in Fig. 2.4.

$$h_c = h_{\max} - h_f + h_{pile} \tag{2-26}$$

Once the contact depth is known, then the area of the contact (A_c) can be calculated and the hardness and elastic modulus determined from the geometry of the indenter. The area function, also sometimes called the indenter shape function, must be carefully calibrated by independent measurements so that deviations from non-ideal indenter geometry are taken into account. For example, for a spherical indenter, the relationship between the contact area (A_c) and the contact depth (h_c) is:

$$A_c = \pi(2Rh_c - h_c^2) \tag{2-27}$$

For a sharp indenters such as Vickers or Berkovich indenter, the relation is:

$$A_c = 24.5 h_c^{\,2} \tag{2-28}$$

Finally, the hardness and elastic modulus are estimated from

$$H = \frac{L_{\max}}{A_c} \tag{2-29}$$

$$E_r = \frac{\sqrt{\pi}}{2}\frac{S}{\sqrt{A_c}} \tag{2-30}$$

2.2.3. Advanced properties

2.2.3.1. Tensile properties

As the spherical indenter penetrates into the sample, the average strain beneath the indenter increases, as does the mean contact pressure. This increase makes it possible to derive the tensile properties of the material by the spherical indentation technique [12-15]. The usual algorithm for obtaining uniaxial stress-strain curve and tensile properties has four steps; step 1 “determination of contact area”, step 2 “defining true stress and strain”, step 3 “fitting to constitutive equation”, and step 4 “evaluation of tensile properties”.

The method to determine the contact depth and area are already mentioned in Sec. 2.2.2. Following Tabor [2]’s approach, the mean pressure can be expressed in a linear relationship with uniaxial true stress as:

$$\sigma_r = \frac{p_m}{\psi} = \frac{1}{\psi}\frac{L}{A_c} \tag{2-31}$$

This relationship is widely used in indentation research and there are many definitions of the plastic constraint factor (ψ) [2, 3]. On the basis of the deformation shape and strain distribution under a spherical indenter, the representative strain are defined using geometric parameter, *a/R*.

$$\varepsilon_r = f(a/R) \tag{2-32}$$

Various researcheres proposed the different ψ value and indentation strain based on the experimental and computational results. Some relations are listed on Table 2.2. The representative stress and strain obtained from instrumented indentation testing (IIT) are fitted using two types of constitutive equations. While a Hollomon-type equation is used for common metallic materials that show power-law hardening, the hardening behavior of austenitic materials can be expressed by a simple linear equation as:

$$\sigma = K\varepsilon^n \tag{2-33}$$

$$\sigma = A + E_T \varepsilon \tag{2-34}$$

where K is the strength coefficient, n is the strain-hardening exponent and E_T is the tangential modulus of material.

Since the elastic modulus can be obtained from IIT, the yield strength (σ_y) can be measured from the intersection point of the flow curve and a line with the slope of the elastic modulus 0.2% offset from the origin. The ultimate tensile strain should be same as the strain-hardening exponent by the theory of instability in tension, and the ultimate tensile strength (σ_u) can be determined. The schematic flow to determine the tensile properties using IIT is shown in Fig. 2.5.

2.2.3.2. Fracture toughness

IIT can be used to evaluate the fracture toughness of materials and interfaces in a similar manner to that conventionally used in larger scale testing. During loading, tensile stresses are induced in the sample material as the radius of the plastic zone increases. Upon unloading, additional stresses arise as the elastically strained material outside the

plastic zone attempts to resume its original shape but is prevented from doing so by the permanent deformation associated with the plastic zone. Ju et al. [16] was modified the critical strain model to evaluate the ductile fracture toughness using the mechanical properties measured from the instrumented indentation tests. The modification of the critical strain model involved: (1) the use of fracture strain from the newly develop model, consisting the stress state, i.e. stress triaxiality, and deformation parameter which can be determined from indentation tests, instead of the critical strain at ahead of crack tip, and (2) the assumption of an empirical calibrated value for the characteristic length, *l**, as the function of the strain hardening exponent [ ]. To determine the fracture strain, he adopted the void growth rate considered in a rigid-perfectly plastic material by Rice and Tracey [ ]. Through its integrating, the fracture strain is given by:

$$\varepsilon_f = ln\left(\frac{R_f}{R_i}\right) / 0.32 exp\left(1.5\frac{\sigma_m}{\bar{\sigma}}\right) \tag{2-35}$$

where R_f and R_i are the final and initial void radius, and σ_m and $\bar{\sigma}$ are the mean normal stress and the equivalent stress, respectively. They has shown experimentally that the ratio of void volume can be expressed by

the reciprocal to the strain hardening exponent. Also ratio of stress is defined as the indentation parameter with regard to deformation. Thus, the critical fracture strain is expressed by:

$$\varepsilon_f = f\left(\frac{1}{n}\right) exp\left(1 - \frac{6A5^n}{\pi \cdot K}\right) \tag{2-36}$$

where A is the material yield parameter. From the relation between the characteristic length and strain hardening exponent [16-18], the modified critical strain model could be defined as:

$$K_{IC} = const.\sqrt{E \cdot \sigma_y \cdot n^2 \cdot f\left(\frac{1}{n}\right) \exp\left(1 - \frac{6A5^n}{\pi \cdot K}\right)} \tag{2-37}$$

where the constant is determined experimentally.

2.2.3.3. Residual stress

Indentation hardness as analyzed from the indentation load and depth curve changes with the material residual stress: indentation load and depth curves are shifted with the direction and magnitude of residual stress within the tested material. However, the variations in the apparent indentation hardness with change in residual stress have been identified as an artifact of erroneous optical measurements of the indentation imprint: in a study of the influence of in-plane stress on indentation plasticity that investigated both the shape of the indentation curve and the contact impressions, the contact hardness was found to be invariant regardless of the elastically applied stress (residual stress) [19-21]. The finite element analysis results showed the important role of sink-in or pile-up deformations around the contact in the stressed state in producing the stress-insensitive contact hardness. Therefore, the change in contact morphologies with residual stress was modeled for constant maximum indentation depth assuming the independence of intrinsic hardness and residual stress.

The change in indentation deformation caused by the residual stress was identified in the indentation loading curve in Fig. 2.6. The applied

load in the tensile-stressed state is lower than that in the stress-free state for the same maximum indentation depth. In other words, the maximum indentation depth desired is reached at a smaller indentation load in a tensile-stressed state because a residual-stress-induced normal load acts as an additive load to the applied load. Therefore, the residual stress can be evaluated by analyzing the residual-stress-induced normal load.

The residual stress is relaxed from a tensile-stressed state to stress-free state while maintaining the constant maximum depth (h_{max}), as the stress relaxation pushes the indenter out from the surface. The pushing force appears as an increase in the applied load ($L_T \rightarrow L_0$) and the contact depth ($h_c^T \rightarrow h_c$), because the maximum depth is held constant. The indentation load and maximum depth for the tensile-stressed state (L_T, h_{max}) are equivalent to those in the relaxed state (L_0, h_{max}). Thus, the relationship between the two states can be expressed as

$$L_0 = L_T + L_{res} \tag{2-38}$$

In the compressive stress state, the applied load and contact depth decrease by stress relaxation under the maximum-depth-controlled path.

Furthermore, this decreasing portion of the applied load was the residual-stress-induced normal load (L_{res}). Therefore, the residual stress in a welded joint can be evaluated by dividing L_{res} by the contact area (A_c) regardless of the stress state:

$$\sigma_{res} = \alpha \frac{L_{res}}{A_c} \tag{2-39}$$

where α is a constant related to the stress directionality of biaxial residual stress. The biaxial stress state, in which $\sigma_y = k\sigma_x$, can be divided into a mean stress term and plastic-deformation-sensitive shear deviator term [19, 21-23]:

Biaxial stress Mean stress Deviator stress

$$\begin{pmatrix} {\sigma^x}_{res} & 0 & 0 \\ 0 & {\sigma^y}_{res} & 0 \\ 0 & 0 & 0 \end{pmatrix} = \begin{pmatrix} \frac{1+k}{3}{\sigma^x}_{res} & 0 & 0 \\ 0 & \frac{1+k}{3}{\sigma^x}_{res} & 0 \\ 0 & 0 & \frac{1+k}{3}{\sigma^x}_{res} \end{pmatrix} + \begin{pmatrix} \frac{2-k}{3}{\sigma^x}_{res} & 0 & 0 \\ 0 & \frac{2-k}{3}{\sigma^x}_{res} & 0 \\ 0 & 0 & -\frac{1+k}{3}{\sigma^x}_{res} \end{pmatrix}$$

(2-40)

The stress component parallel to the indentation axis in the deviator

stress term directly affects the indenting plastic deformation. A residual-stress-induced normal load L_{res} can be defined from the selected deviator stress component as:

$$L_{res} = \frac{1+k}{3}\sigma_{res}A_c \tag{2-41}$$

Therefore, k in Eq. (2-41) can be taken as approximately 1.0 in the thin-film system (equivalent-biaxial stress state) and 3.0 in the welded zone. In the instrumented indentation test, the contact area is determined by unloading curve analysis. By differentiation of the power-law-fitted unloading curve at maximum indentation depth, the contact depth and contact area can be calculated from the contact depth based on the geometry of the Vickers indenter as:

$$A_c = 24.5h_c^{\,2} \tag{2-42}$$

Thus, residual stress was calculated from the analyzed contact area in Eq. (2-42) and the measured load change L_{res} by the effect of residual stress in Eq. (2-14).

Table 2.1. Elastic solution for various indenters (taking $\upsilon = 0.5$)

	Wedge	Cone	Cylinder	Sphere
Mean pressure (P_m)	$\frac{E\tan\theta}{2(1-\upsilon^2)}$	$\frac{E\tan\theta}{2(1-\upsilon^2)}$	$\frac{\pi}{8}\frac{E(a/R)}{(1-\upsilon^2)}$	$\frac{4}{3\pi}\frac{E(a/R)}{(1-\upsilon^2)}$
Pressure distribution ($p(x)$ or $p(r)$)	$\frac{2P_m}{\pi}$ arcosh(a/x)	P_m arcosh(a/x)	$\frac{4P_m}{\pi}(1-a^2/x^2)^{1/2}$	$\frac{3P_m}{2}(1-a^2/x^2)^{1/2}$
Maximum shear stress (τ)	$\frac{2P_m}{\pi}$ at (0,0)	P_m at (0,0)	$0.38P_m$ at (0,78a)	$0.47P_m$ at (0,48a)
Pressure for first yield	$0.97\sigma_y$	$0.5\sigma_y$	$1.5\sigma_y$	$1.1\sigma_y$

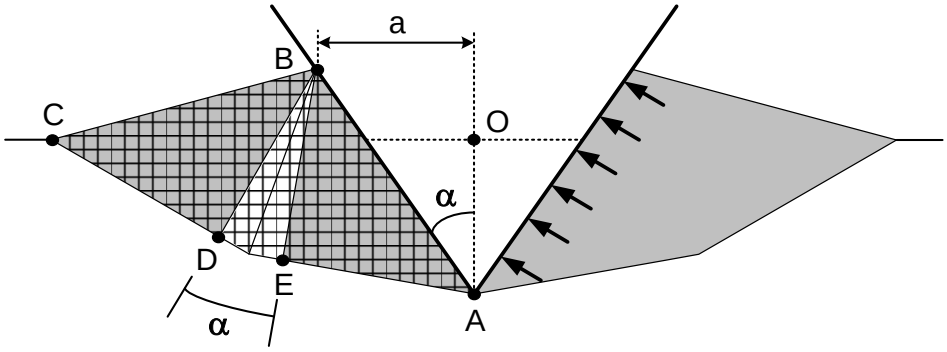

Figure 2.1. Slip-line theory [2].

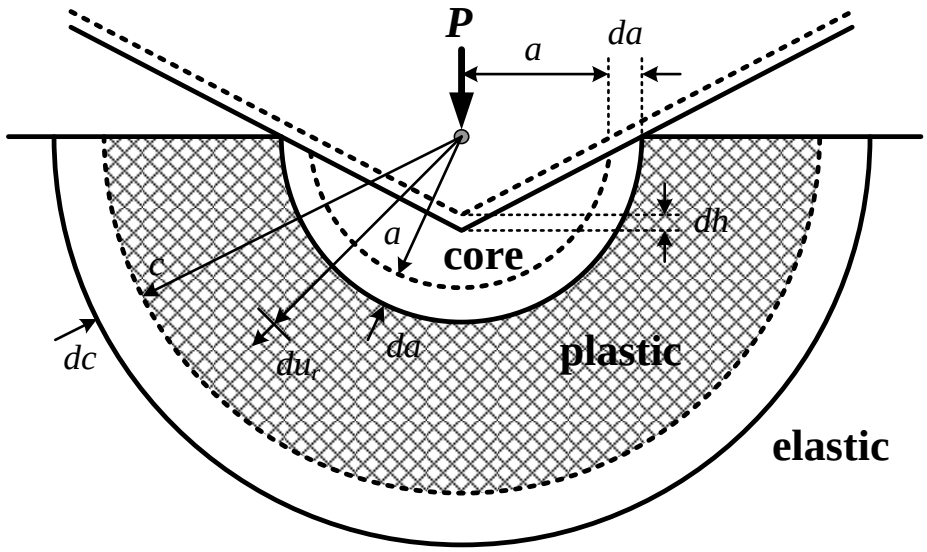

Figure 2.2. Schematic diagram of expanding cavity model [2, 24].

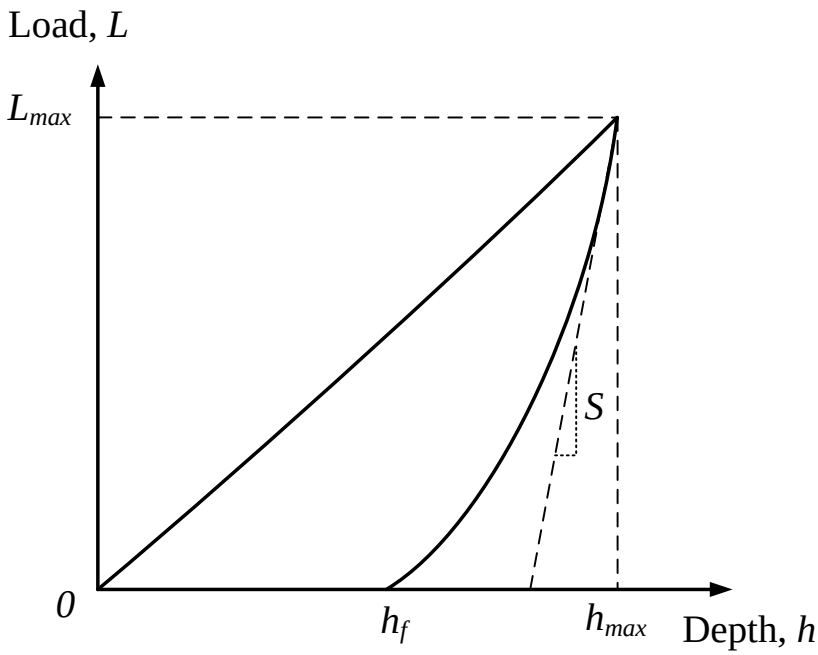

Figure 2.3. Schematic diagram of load and depth curve obtained by spherical indentation.

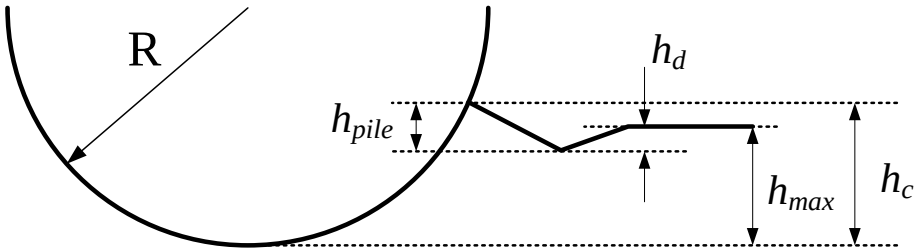

Figure 2.4. Cross section of contact morphology in the loaded state by a spherical indenter.

Table 2.2. Definitions of constraint factor and indentation strain.

	ψ	Indentation strain
D. Tabor (1950)	3	$0.2\frac{a}{R}$
J.R. Matthew (1980)	$\psi = \frac{6}{2+n}\left(\frac{40}{9\pi}\right)^n$	$\left(\frac{2n}{2n+1}\right)^n \frac{8}{9\pi}\frac{a}{R}$
B. Taljat (1998)	$\psi = -0.81 + \frac{2}{\sqrt{n+0.2}}$	$0.2\frac{a}{R}$
J.H. Ahn & D. Kwon (2000)	3	$0.14\frac{a}{R-h_c}$
G. Sundararajan (2006)	$\psi = 0.133 \cdot \frac{\beta^3}{1+0.25n}$	$0.2\frac{a}{R}$

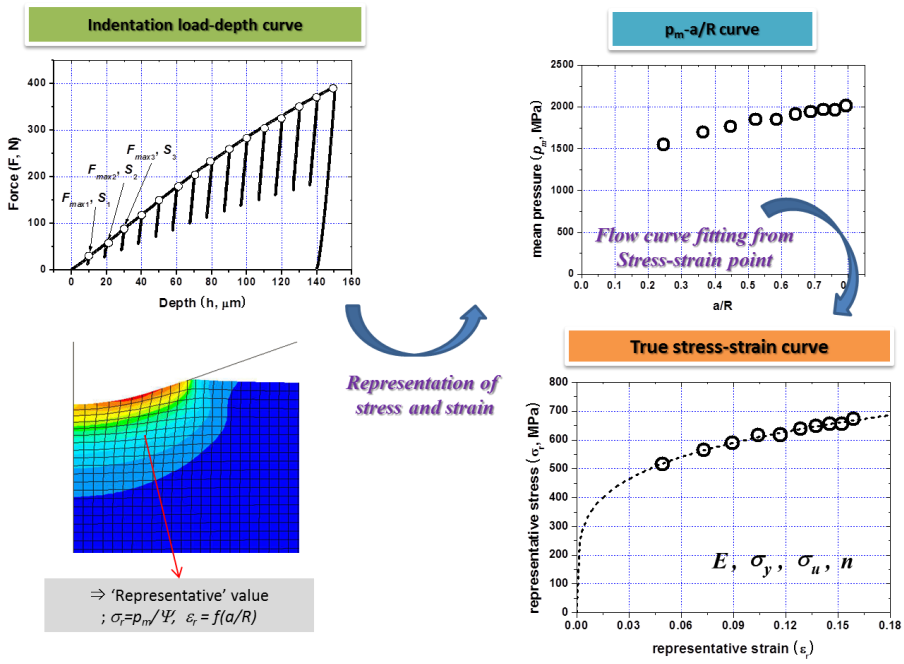

Figure 2.5. Schematic flow of evaluating tensile properties using IIT .

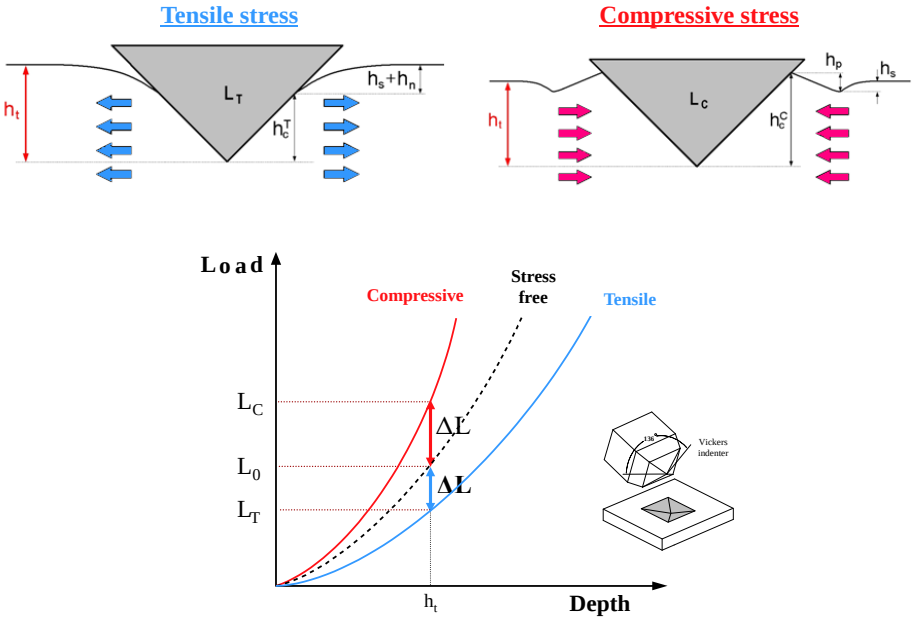

Figure 2.6. Basic principle of residual stress measurement using IIT.

References

[1] E. Meyer, Investigations of hardness testing and hardness, Phy. Z. 9 (1908) 66-74.

[2] D. Tabor, The hardness of metals, Clarendon, Oxford, 1951.

[3] R. Hill, The mathematical theory of plasticity, Clarendon, Oxford 613 (1950) 614.

[4] H. Lee, J. Haeng Lee, G.M. Pharr, A numerical approach to spherical indentation techniques for material property evaluation, Journal of the Mechanics and Physics of Solids 53(9) (2005) 2037-2069.

[5] D. Marsh, Plastic flow in glass, Proceedings of the Royal Society of London. Series A. Mathematical and Physical Sciences 279(1378) (1964) 420-435.

[6] K.L. Johnson, The correlation of indentation experiments, Journal of the Mechanics and Physics of Solids 18(2) (1970) 115-126.

[7] L. Samuels, T. Mulhearn, An experimental investigation of the deformed zone associated with indentation hardness impressions, Journal of the Mechanics and Physics of Solids 5(2) (1957) 125-134.

[8] W.C. Oliver, G.M. Pharr, An improved technique for determining

hardness and elastic modulus using load and displacement sensing indentation experiments, Journal of materials research 7(6) (1992) 1564-1583.

[9] Y.-T. Cheng, C.-M. Cheng, Scaling, dimensional analysis, and indentation measurements, Materials Science and Engineering: R: Reports 44(4) (2004) 91-149.

[10] A. Giannakopoulos, S. Suresh, Determination of elastoplastic properties by instrumented sharp indentation, Scripta materialia 40(10) (1999) 1191-1198.

[11] J. Alcalá, A.C. Barone, M. Anglada, The influence of plastic hardening on surface deformation modes around Vickers and spherical indents, Acta Materialia 48(13) (2000) 3451-3464.

[12] J.-H. Ahn, D. Kwon, Derivation of plastic stress–strain relationship from ball indentations: Examination of strain definition and pileup effect, 2001.

[13] J.-H. Ahn, E.-c. Jeon, Y. Choi, Y.-H. Lee, D. Kwon, Derivation of tensile flow properties of thin films using nanoindentation technique, Current Applied Physics 2(6) (2002) 525-531.

[14] S.-H. Kim, Y. Choi, D.-I. Kwon, Determination of Brinell Hardness through Instrumented Indentation Test without Observation of Residual

Indent, 2004.

[15] S.-H. Kim, E.-c. Jeon, D. Kwon, Determining Brinell Hardness From Analysis of Indentation Load-Depth Curve Without Optical Measurement, 2005.

[16] J.-B. Ju, W.-s. Kim, J.-i. Jang, Variations in DBTT and CTOD within weld heat-affected zone of API X65 pipeline steel, Materials Science and Engineering: A 546 (2012) 258-262.

[17] S.-W. Jeon, K.-W. Lee, J.Y. Kim, W.J. Kim, C.-P. Park, D. Kwon, Estimation of Fracture Toughness of Metallic Materials Using Instrumented Indentation: Critical Indentation Stress and Strain Model, Experimental Mechanics 57(7) (2017) 1013-1025.

[18] J.-S. Lee, J.-i. Jang, B.-W. Lee, Y. Choi, S.G. Lee, D. Kwon, An instrumented indentation technique for estimating fracture toughness of ductile materials: A critical indentation energy model based on continuum damage mechanics, Acta Materialia 54(4) (2006) 1101-1109.

[19] M.-J. Choi, S.-K. Kang, I. Kang, D. Kwon, Evaluation of nonequibiaxial residual stress using Knoop indenter, Journal of Materials Research 27(1) (2012) 121-125.

[20] L. Xiao, D. Ye, C. Chen, A further study on representative models for calculating the residual stress based on the instrumented indentation

technique, Computational Materials Science 82 (2014) 476-482.

[21] Y.-C. Kim, M.-J. Choi, D. Kwon, J.-Y. Kim, Estimation of principal directions of Bi-axial residual stress using instrumented Knoop indentation testing, Metals and Materials International 21(5) (2015) 850-856.

[22] H.-J. Ahn, J.-h. Kim, H. Xu, J. Lee, J.-Y. Kim, Y.-C. Kim, D. Kwon, Directionality of residual stress evaluated by instrumented indentation testing using wedge indenter, Metals and Materials International 23(3) (2017) 465-472.

[23] J.-h. Kim, H. Xu, M.-J. Choi, E. Heo, Y.-C. Kim, D. Kwon, Determination of directionality of nonequibiaxial residual stress by nanoindentation testing using a modified Berkovich indenter, Journal of Materials Research (2018) 1-8.

[24] S.-K. Kang, Y.-C. Kim, K.-H. Kim, J.-Y. Kim, D. Kwon, Extended expanding cavity model for measurement of flow properties using instrumented spherical indentation, International Journal of Plasticity 49 (2013) 1-15.

Chapter 3

EVALUATION OF INDENTATION YIELD STRENGTH FOR ANISOTROPIC MATERIALS

Contents

3.1. Motivation and Research Flow

As mentioned in Chapter 1 and 2, many studies [1-5] were conducted to evaluate the yield strength of metallic materials using the spherical indentation. Typically, the modified Meyer relation [4] can be used to the indentation yield strength using the spherical indentation, which are discussed in detail in Chapter 4. That is, the indentation yield strength from modified Meyer relation can be calculated by multiplying the material-type constant related to the strain-hardening behavior and the Meyer constant. As such, experimental or theoretical studies have been carried out to determine the material yield strength using various indenters such as spherical and Vickers indenters. However, axisymmetric shaped indenters have limitation in that it cannot sense the direction of yield strength. In addition, the modified Meyer relation [4] does not take into account the directionality of mechanical properties such as the yield strength, elastic modulus and strain-hardening exponent.

Here, we attempted to derive an indentation yield strength model considering directionality of yield strength for the application of plastic deformation in one direction, such as cold rolling process. Several

dimensionless functions based on both indentation load and depth curve and directionality were established to correlate the indentation response with material constitutive parameters. In order to obtain basic data of modeling, finite element simulations were conducted using the imaginary materials which were made by changing yield strength, directional ratio of yield strength and strain-hardening exponent. Spherical indentation tests were performed on these imaginary materials, and a model was established based on Buckingham′s PI-theorem [6-8], one of the dimensional analyzes, using the data set related to the indentation response.

As mentioned above, since same indentation curve are obtained even if the axisymmetric indenter is rotated around the indenting axis, the directionality of yield strength cannot be obtained from the axisymmetric indenter alone. On the other hand, the indentation deformation around the residual impression is not axisymmetric for materials with mechanical anisotropy. The indentation surface displacement caused by indentation will be affected by the mechanical anisotropy, and if we can quantitatively evaluate the surface displacement, we can infer the mechanical anisotropy from it. By introducing this phenomenal concept,

we tried to obtain information on the directionality of yield strength from the surface deformation around residual impression. In order to determine the direction ratio of yield strength included the model, a surface displacement distribution around the impression was analyzed based on the finite element simulation. The displacement change in the x- and y-axis around the impression was analyzed depending on various direction ratio of yield strength, and it was confirmed how the relationship between the direction ratio of yield strength and that of the displacement was affected by tensile properties.

For the results obtained by simulation data, experimental verification was performed with Digital Image Correlation (DIC) method. Generally, the surface deformation is measured by a strain gauge, which is widely used in uniaxial tensile or compression testing; however, the strain gauge has the limitation that only one strain value can be measured by one strain gauge. In addition to the strain gauge, there are methods using electron speckle pattern interferometry (ESPI) to measure surface deformation. However, we chose the digital image correlation method here because its results can be analyzed from macro- to nanoscale, an attractive feature to combine with indentation′s advantage of multi-scale

testing. After obtaining images of the testing area before and after spherical indentation using the DIC imaging system, displacements by indentation around the residual impression can be evaluated by comparing the two images. 3D digital image correlation also lets us evaluate indentation pileup or sink-in; however, 2D digital image correlation was used here only to evaluate displacements parallel to the surface for convenience in testing. The flow of this study can be seen in Fig. 2.

3.2. Evaluation of indentation yield strength considering directionality

3.2.1 Theoretical modeling

Since indentation measurements have been applied to a great variety of materials, ranging from metals, ceramics, polymers, it is necessary to model indentation using general though simplified descriptions for the mechanical properties of solids, including the yield strength, elastic modulus and strain-hardening exponent, etc [8-10]. Dimensional analysis is then used to explore various aspects of indentation in these model systems with the aid of finite element analysis when necessary [6]. The essential idea of dimensional analysis is that physical law do not depend on arbitrarily chosen basic units of measurement. Consequently, the functions expressing physical laws must process certain mathematical property, and each of the additive terms in the functions will have the same dimensions or units. This property allows the number of arguments in the mathematical expressions to be reduced, thus making them simpler to obtain either from theories or experiments. The basic idea leads to the

central theorem in dimensional analysis, the so-called PI-theorem (or Π -theorem), which has been attributed to Buckingham.

Many studies [6] provide the following recipe for dimensional analysis:

(1) Listing independent variable and parameters that the quantity of interest depends on. There should be a relationship for each dependent quantity.

(2) Identifying independent variables and parameters with independent dimensions.

(3) Forming dimensionless quantities and establishing relationships among dimensionless quantities. The number of relationships is equal to the number of dependent quantities.

For the indentation loading curve of a spherical indentation, various dimensional functions using the PI-theorem have already been proposed to derive elasto-plastic properties for the isotropic materials [8]. On the other hand, this study considers anisotropic plasticity, and therefore we need to include an anisotropic parameter in the dimensional function. Referring to previous works [8-10], the loading data can be expressed by the following Π_1-function.

$$F = \prod_1 \left(\sigma_{Yx}, E, m, \upsilon, n, h, R \right) \tag{1}$$

where σ_{Yx} is the yield strength of x-axis, E is the elastic modulus, m is the directional ratio of yield strength $\left(\sigma_{Yy} / \sigma_{Yx} \right)$, n is the strain-hardening exponent, h is the indentation depth and R is the indenter radius. Applying Buckingham's PI-theorem to Eq. (1) to make a dimensionless term is as follows:

$$\pi_1 = E^{a_1} h^{b_1} F = [FL^{-2}]^{a_1} [L^1]^{b_1} [F^1] = [F^0 L^0] \tag{2}$$

$$\rightarrow \pi_1 = E^{-1} h^{-2} F = \frac{F}{Eh^2}$$

As in Eq. (1), the remaining terms are as follows:

$$\pi_2 = \frac{\sigma_{Yx}}{E}, \ \pi_3 = m, , \ \pi_4 = \upsilon, \ \pi_5 = n, \ \pi_6 = \frac{h}{R} \tag{3}$$

And, the dimensionless function ($\prod_2$) considering the directional ratio of yield strength is as follows:

$$\frac{F}{Eh^2} = \prod_2 \left(\frac{\sigma_{Yx}}{E}, m, \upsilon, n, \frac{h}{R} \right) \tag{4}$$

The following assumption and condition were considered in this study to derive a simple function of evaluating yield strength at each direction. (1) Elastic modulus and Poisson's ratio of common metals was used as E = 200 GPa and $\upsilon = 0.3$. (2) Only the anisotropy of yield strength was considered as $m = \sigma_{Yy} / \sigma_{Yx}$. (3) All indentation parameters were obtained at $h/R = 0.56$. Considering the above assumptions and condition, Eq. (4) is summarized to be simplified dimensionless function ($\prod_3$) as follows:

$$\frac{F}{Eh^2} = \prod_3 \left(\frac{\sigma_{Yx}}{E}, m, n \right) \tag{5}$$

If the variables F / Eh^2, E, m and n are determined, we can define the unknown variable σ_{Yx}. In order to derive a relationship between these dimensionless terms, we conducted finite element simulation using ABAQUS 6.14 version for the spherical indentation, and the data set of

material properties can be seen in Table. 3.1. The spherical indenter with a radius of 150 μm was designed as a discrete rigid type and consists of 969 elements of the R3D4 type. Cubic sample with size of $45 \times 40 \times 20$ mm was designed as a 3D deformable type of C3D8 and consists of 31,494 elements. Interaction was surface-to-surface contact type and friction coefficient was considered by 0.1. Figure 3.3 shows the spherical indentation simulated using above conditions in ABAQUS. As shown in Fig. 3.4, the spherical indentation model shows good agreement between indentation load and depth curve from finite element simulation and that of experiment for S20C.

First, the relationship between F/Eh^2 and m was confirmed by changing the yield strength of x-axis and the strain-hardening exponent for a fixed elastic modulus. As shown in Fig. 3.5, the dimensionless terms F/Eh^2 and m have a linear relationship depending on n and σ_{Yx}/E. As the yield strength of x-axis and strain-hardening exponent increased, the slope (α) and intercept (β) of the fitted line between F/Eh^2 and m increased. The detailed fitting constants are summarized in Table 3.2, and we obtained the linear function of $F/Eh^2 = f(m)$ for each σ_{Yx}/E and n.

Second, to reflect the yield strength of x-axis in the dimensionless function, the relationship between α, β and σ_{Yx} / E was confirmed for each imaginary materials. Figure 3.6 shows the relationship between α, β and σ_{Yx} / E for each the strain-hardening exponent. The slope a_1 and intercept a_2 for α and the slope b_1 and intercept b_2 for β are summarized in the Table 3.3.

Finally, we obtained the following simplified formula for each strain-hardening exponent.

$$\frac{F}{Eh^2} = \left(a_1 \cdot \frac{\sigma_{Yx}}{E} + a_2 \right) \cdot m + \left(b_1 \cdot \frac{\sigma_{Yx}}{E} + b_2 \right) \tag{6}$$

And, Eq. (6) can be derived for σ_{Yx} as follows.

$$\sigma_{Yx} = \left(\left(\frac{F}{Eh^2} - a_2 \cdot m - b_2 \right) \cdot \frac{1}{a_1 \cdot m - b_1} \right) \cdot E \tag{7}$$

In equation (7), *F* and *h* can be obtained from the spherical indentation loading curve, and *E* can be determined by the Oliver and Pharr method.

And if *m* is determined, yield strength of the x-axis can be calculated.

3.2.2 Computational verification

The spherical indentation loading curve obtained from finite element simulation was used to verifying the suggested equation (7) by dimensional analysis in Sec. 3.2.1. We confirmed the relative error between the input yield strength of the x-axis and the yield strength of the x-axis calculated from Eq. (7), and these results are summarized in Fig. 3.7. It can be confirmed that the estimated results match well within 10% of the relative error. Therefore, this indentation model suggested in this study seems to have a good combination of indentation parameters and mechanical properties. As the next step, the evaluation method for *m* in Eq. (7) was explained in Sec. 3.3.

3.3. Evaluation of directionality of yield strength

3.3.1 Phenomenological modeling

Previous works [11-13] proposed a method for directly determining anisotropic plastic properties using indentation response. When a spherical indenter is impressed against in-plane anisotropic materials, the impression geometry is found to form an anisotropic shape. Inspired by this, the functional relationship between anisotropic plastic properties and indentation responses including impression geometry were explored based on a parametric finite element simulation study. Yonezu et al. [8] confirmed that pile-up height around the impression is strongly dependent on the orthotropic axis; That is, the pile-up height for the y-direction (T-direction) is higher than that for the x-direction (L-direction) for an SiC whisker-reinforced aluminum alloy. This can be attributed to the anisotropic properties of the composite, since the plastic flow stress along the L-direction is higher than that along the T-direction. Like this, many studies have proposed an anisotropy evaluation method using indentation contact morphology around the spherical indentation such as

plastic pile-up or sink-in. However, deformations that occur in the z-axis, such as plastic pile-up or sink-in, cannot be measured with simple equipment, and cannot be measured in the field. Therefore, in order to overcome this limitation, we tried to correlate the anisotropy with the in-plane displacement behavior around spherical indentation. The basic concept of this phenomenological modeling is shown in Fig 3.8. The isotropic material will have the same displacement distribution around indentation in the x and y directions. On the other hand, anisotropic materials will have different displacement distribution in the x and y directions. Using this basic concept, displacement changes in the x and y directions before and after indentations were analyzed for all imaginary materials. As shown in Fig. 3.9, in order to quantify the directionality, the displacement change occurring around the spherical indentation was obtained in the x and y directions corresponding to the same position from the zero point.

Figure 3.11 shows the results of displacement lines in the x- and y-axis as the yield strength changes in the x-axis. Here, as shown in Fig. 3.10, we assumed that the further away from the spherical indentation, the deformation decreases and becomes zero. Therefore, we fitted the

linear lines of D_x and D_y past the origin. From this approach, it can be seen that as the directional ratio of yield strength increases, the slope of the linear line of D_x and D_y decreases. Figure 3.12 shows the results of displacement lines in the x- and y- axis as the strain-hardening exponent. It also can be seen that as the directional ratio of yield strength increases, the slope of the linear line of D_x and D_y decreases. Using this phenomenon, we performed modeling to evaluate the directional ratio of yield strength.

Figure 3.13 shows the relationship between the linear line slope (*a*) of D_x and D_y and the directional ratio of yield strength depending on the yield strength of x-axis and strain-hardening exponent. It can be seen that the slope is independent of yield strength of x-axis and strain-hardening exponent. Therefore, the following phenomenological model can be derived.

$$a = 1.00 \cdot m\left(=\frac{\sigma_{Yy}}{\sigma_{Yx}}\right)^{-3.05} \tag{8}$$

3.3.2 Experimental and computational verification

In order to verify the proposed method, As-received STS304L, 10% cold rolled STS304L, 20% cold rolled STS304L, as-received S20C and STS410 samples were prepared. Spherical indentation tests were performed at a maximum indentation depth of 150 μm using AIS3000 instrument (FRONTICS, Republic of Korea). Images of the testing area were taken before and after the indentation using a camera system (Fig. 3.14) and displacement information was calculated using digital image correlation software developed by Prof. Schajer at The University of British Columbia. And, the displacement analysis conditions are specified in Fig. 3.15. The software makes it possible to analyze *x*-displacement, *y*-displacement, radial displacement, and hoop displacement.

The proposed model was verified for as-received STS304L, as-received S20C and as-received STS410. Figure 3.16 shows the results of surface displacement around the spherical indentation for three materials. From these results, it can be seen that the displacement in the direction with larger yield strength occurs less. From the DIC results, we measured the displacement slope *a* of x- and y-axis (Fig. 3.17). For as-received

samples, we can see that the displacement slope *a* is close to 1. On the other hand, we can confirm that the displacement slope *a* decreases as the cold rolling rate increases (Fig. 3.18 and 19). Using Eq. (8) and surface displacement results, directional ratio of yield strength was estimated and compared to directional ratio obtained from the uniaxial tensile test. Figure 3.20 shows the comparison result of the estimated directional ratio of yield strength and that of uniaxial tensile test for as-received, 10% cold rolled and 20% cold rolled STS304L. From this result, it can be confirmed that equation (8) shows good agreement.

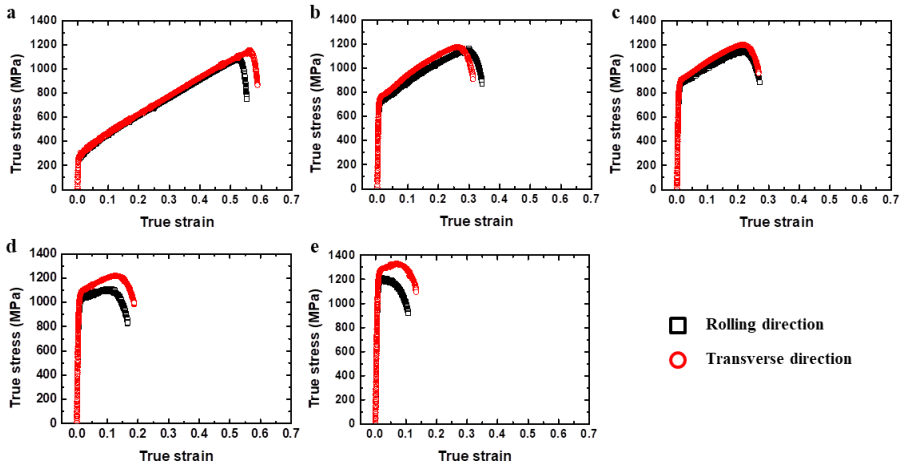

Figure 3.1 True stress and strain curves of STS 304L for cold rolling direction and transverse direction

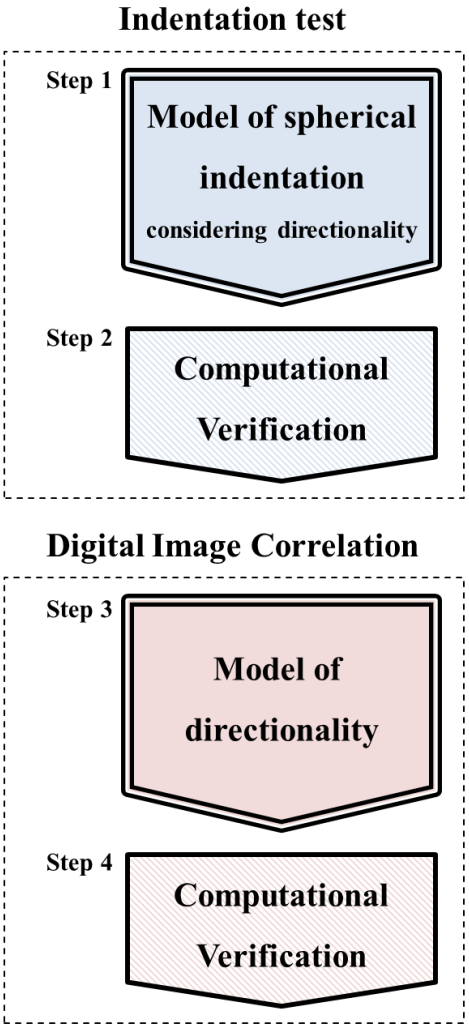

Figure 3.2 Flow chart of deriving model of indentation yield strength considering directionality

Table 3.1. Data set of materials properties for imaginary materials in FEA simulation

σ_{Yx} (MPa)	n	$m\left(=\sigma_{Yy}/\sigma_{Yx}\right)$			
265	0.2	1	1.2	1.4	1.6
	0.3	1	1.2	1.4	1.6
	0.35	1	1.2	1.4	1.6
	0.4	1	1.2	1.4	1.6
	0.45	1	1.2	1.4	1.6
350	0.2	1	1.2	1.4	1.6
	0.3	1	1.2	1.4	1.6
	0.35	1	1.2	1.4	1.6
	0.4	1	1.2	1.4	1.6
	0.45	1	1.2	1.4	1.6
450	0.2	1	1.2	1.4	1.6
	0.3	1	1.2	1.4	1.6
	0.35	1	1.2	1.4	1.6
	0.4	1	1.2	1.4	1.6
	0.45	1	1.2	1.4	1.6
550	0.2	1	1.2	1.4	1.6
	0.3	1	1.2	1.4	1.6
	0.35	1	1.2	1.4	1.6
	0.4	1	1.2	1.4	1.6
	0.45	1	1.2	1.4	1.6
650	0.2	1	1.2	1.4	1.6
	0.3	1	1.2	1.4	1.6
	0.35	1	1.2	1.4	1.6
	0.4	1	1.2	1.4	1.6
	0.45	1	1.2	1.4	1.6

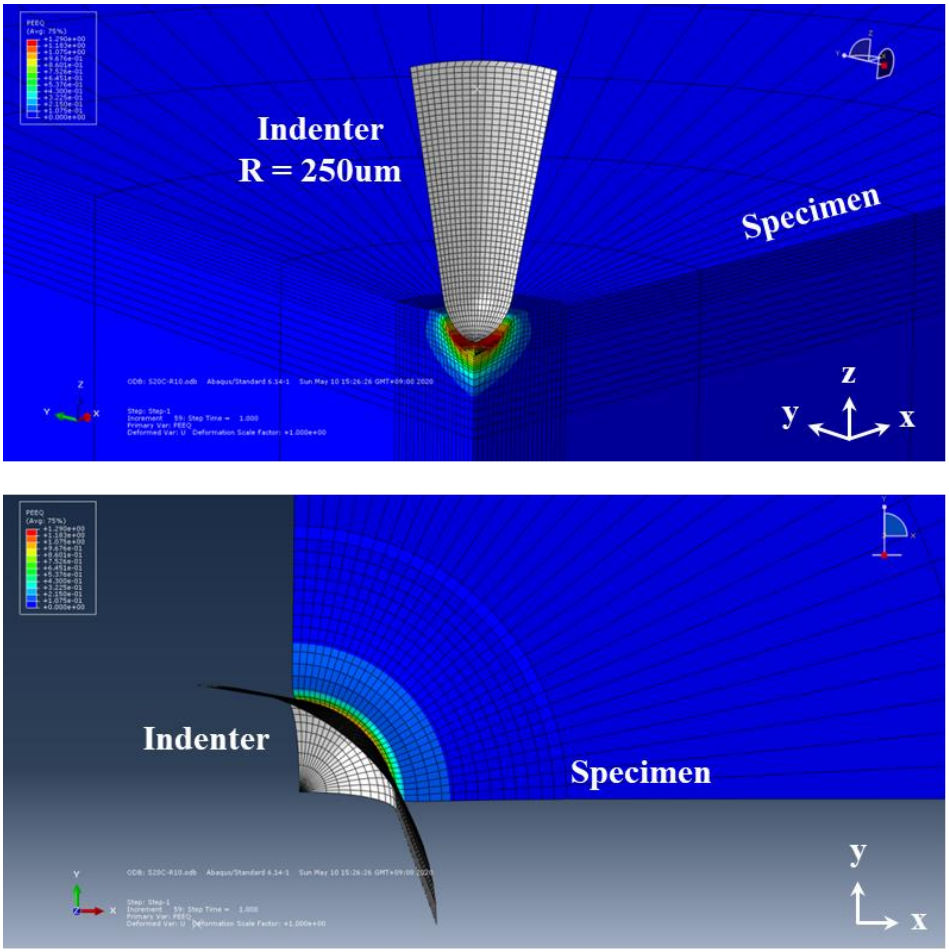

Figure 3.3. Spherical indentation simulated using ABAQUS

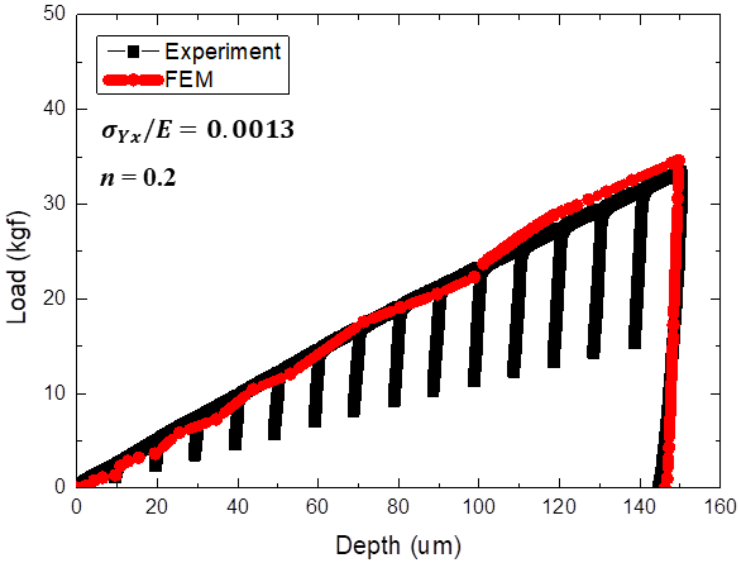

Figure 3.4. Comparison of indentation curves obtained from experiment and finite element simulation for S20C

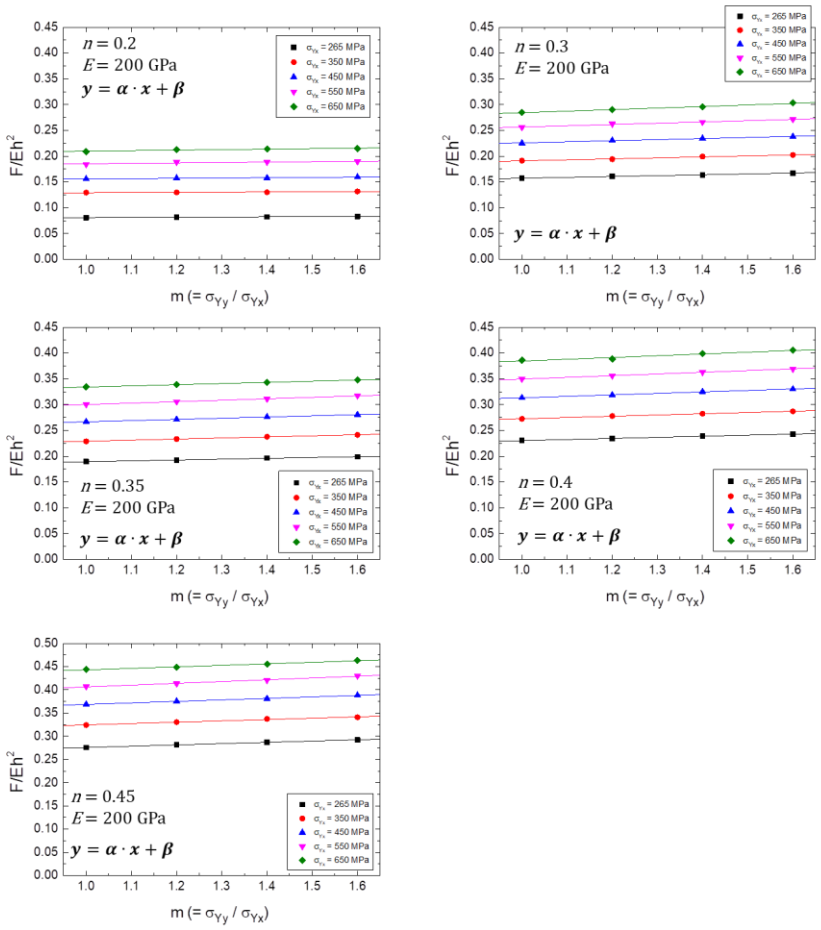

Figure 3.5. Relationship between F / Eh^2 and m for each yield strength and strain-hardening exponent

Table 3.2. Results of relationship between $\mathrm{F}/\mathrm{E}h^2$ and m for each yield strength and strain-hardening exponent

n	σ_{Yx} / E	α	β
0.2	0.0013	0.0033	0.0779
	0.0018	0.0036	0.1256
	0.0023	0.0058	0.1502
	0.0028	0.0080	0.1773
	0.0033	0.0091	0.2010
0.3	0.0013	0.0165	0.1409
	0.0018	0.0191	0.1720
	0.0023	0.0211	0.2047
	0.0028	0.0251	0.2313
	0.0033	0.0265	0.2584
0.35	0.0013	0.0162	0.1733
	0.0018	0.0210	0.2081
	0.0023	0.0231	0.2437
	0.0028	0.0279	0.2723
	0.0033	0.0297	0.3114
0.4	0.0013	0.0211	0.2092
	0.0018	0.0245	0.2480
	0.0023	0.0283	0.2850
	0.0028	0.0324	0.3174
	0.0033	0.0328	0.3509
0.45	0.0013	0.0275	0.2484
	0.0018	0.0288	0.2958
	0.0023	0.0323	0.3363
	0.0028	0.0385	0.3677
	0.0033	0.0396	0.4104

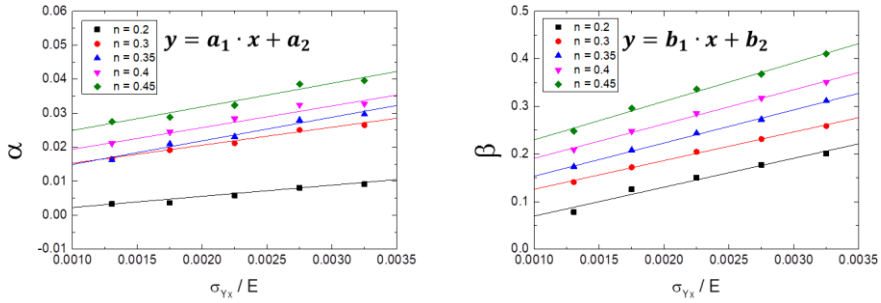

Figure 3.6. Relationship between α, β and σ_{Yx}/E for strain-hardening exponent

Table 3.3. Results of relationship between α, β and σ_{Yx}/E for strain-hardening exponent

n	a_1	a_2	b_1	b_2
0.2	3.277	-0.001	60.671	0.009
0.3	5.290	0.010	60.092	0.066
0.35	4.042	0.013	69.566	0.084
0.4	6.376	0.013	72.014	0.119
0.45	4.039	0.023	80.788	0.149

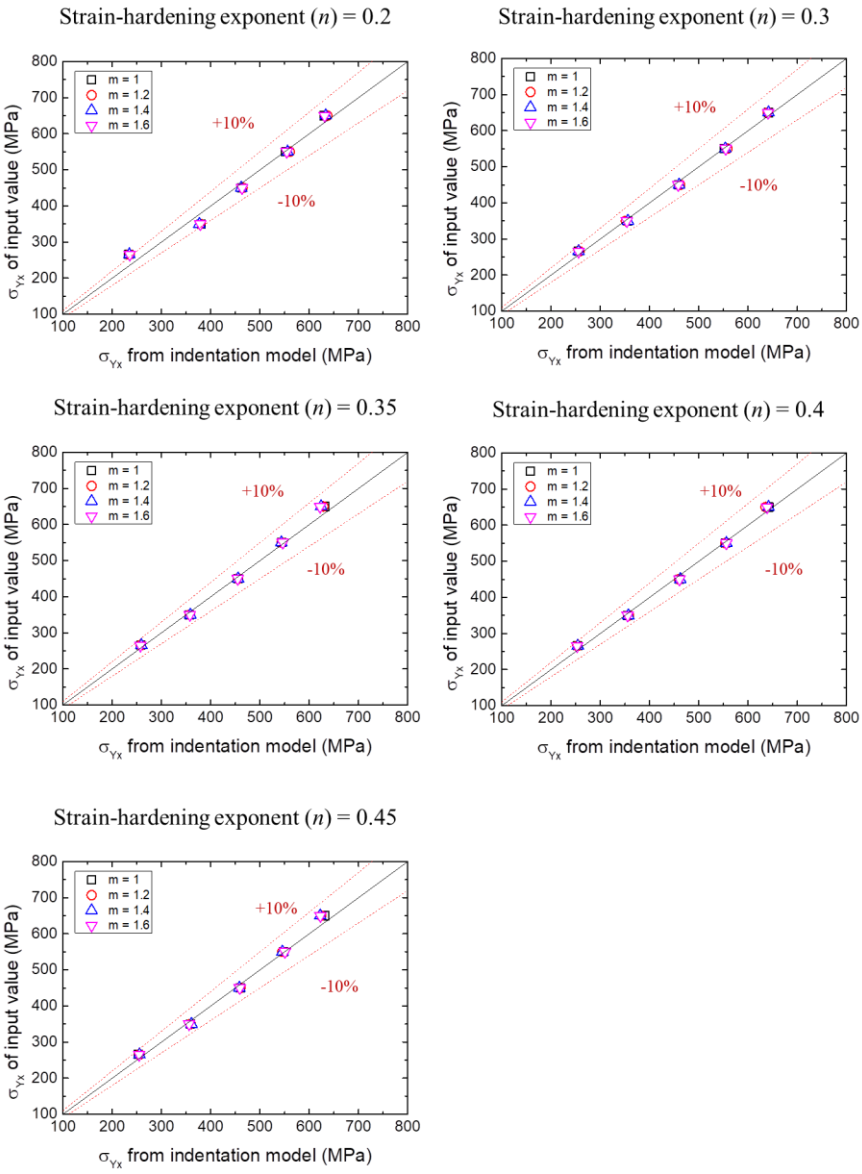

Figure 3.7. Results of estimated yield strength by yield strength ratio (*m*)

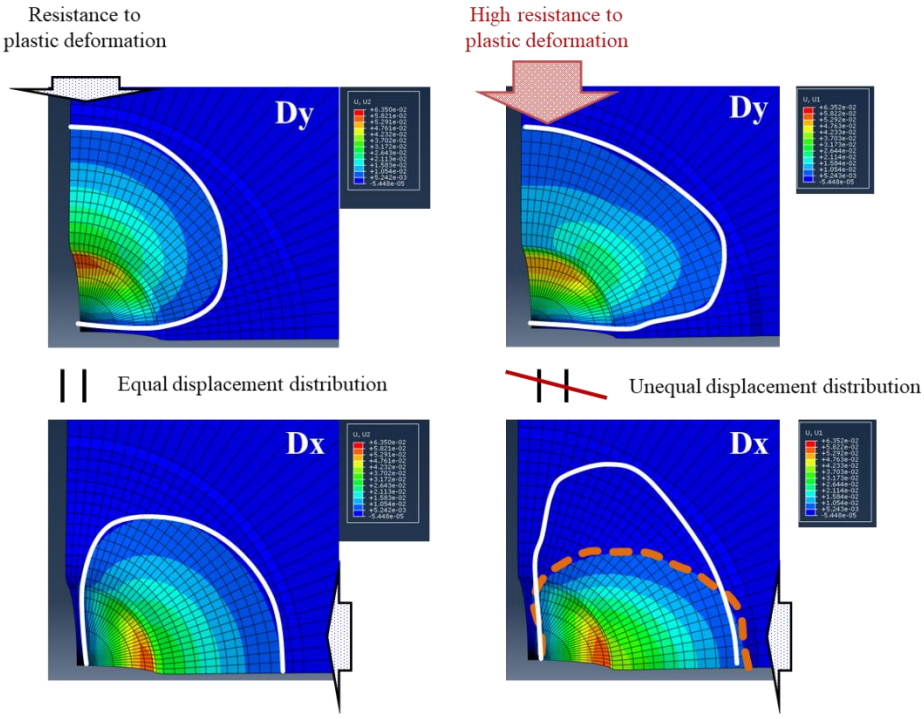

Figure 3.8. Basic concept of evaluating yield strength ratio (*m*)

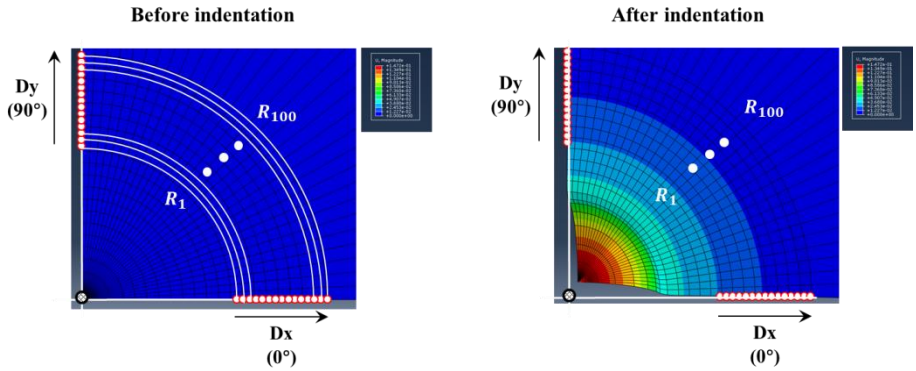

Figure 3.9. Quantification method of directionality using surface displacement around spherical indentation

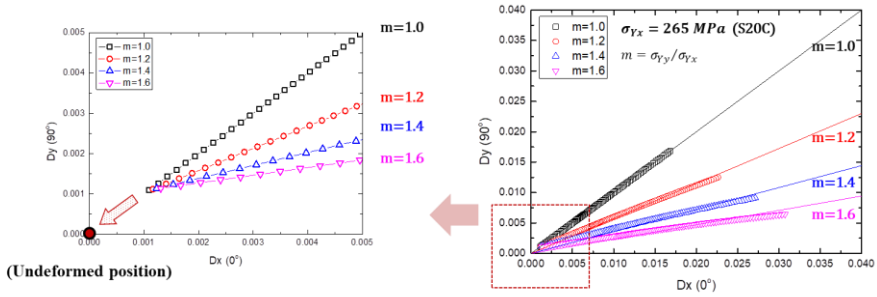

Figure 3.10. Fitting lines of D_x and D_y past the origin

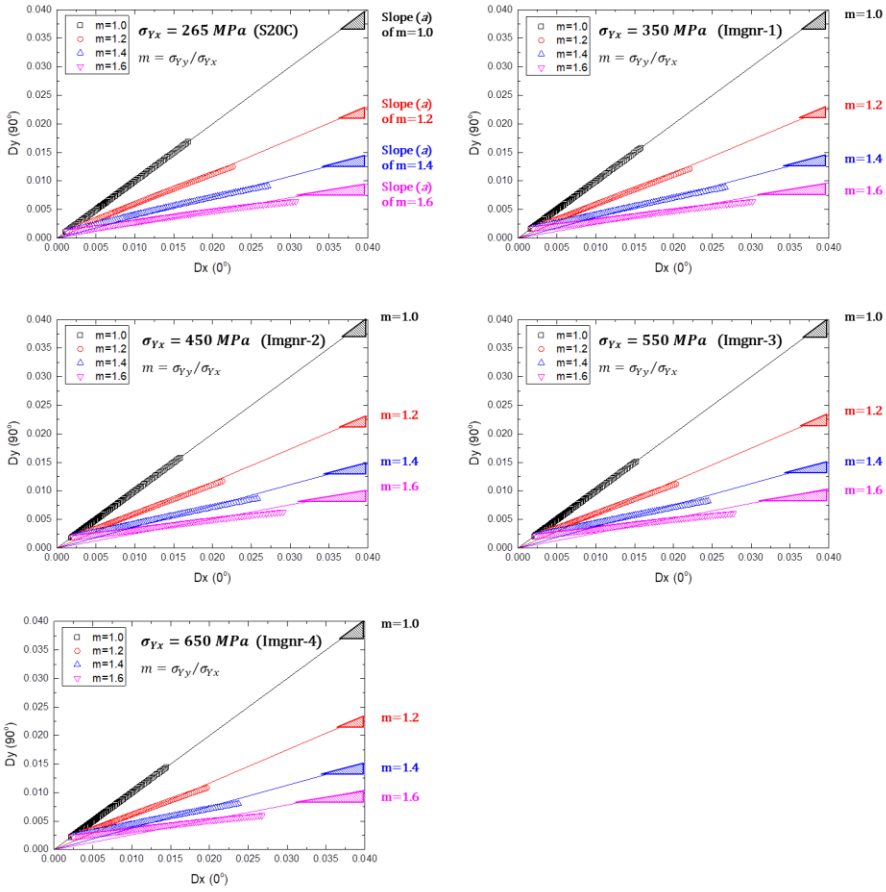

Figure 3.11. Results of displacement for x and y direction depending on yield strength of x-axis

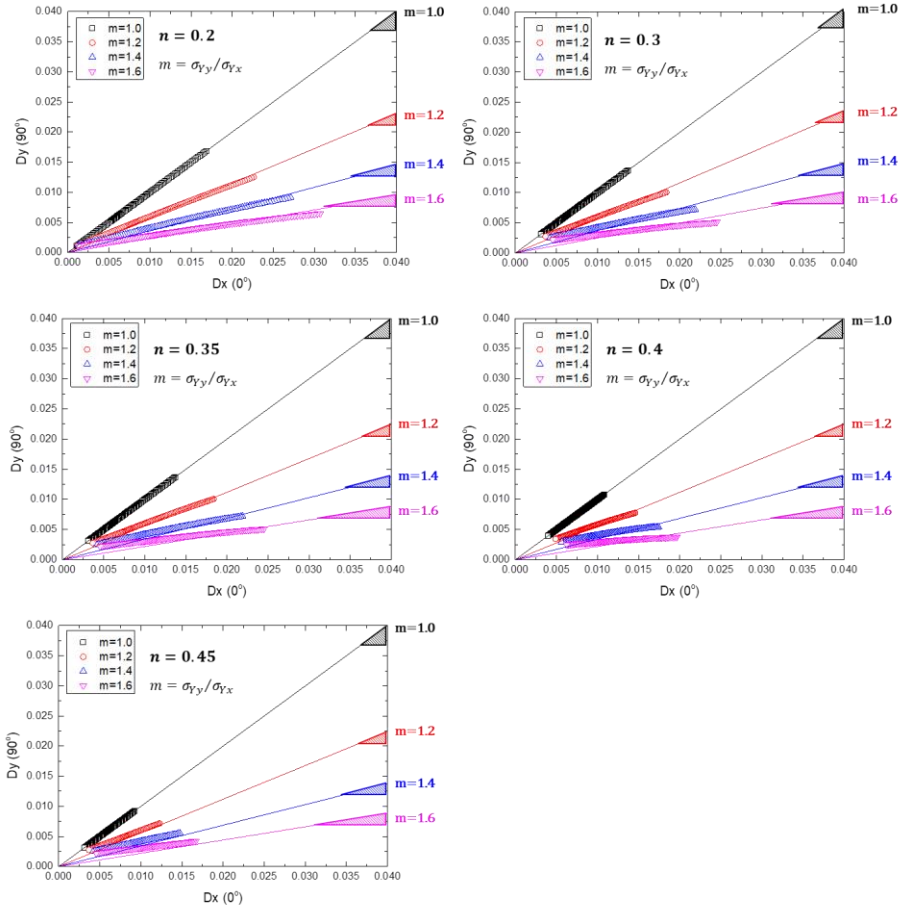

Figure 3.12. Results of displacement for x and y direction depending on strain-hardening exponent

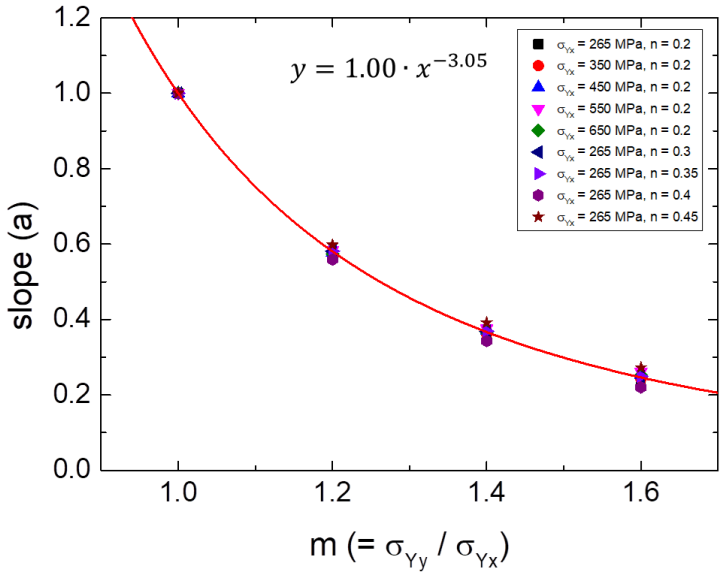

Figure 3.13. Comparison of displacement line slope (*a*) and yield strength ratio (*m*) depending on yield strength of x-axis and strain-hardening exponent

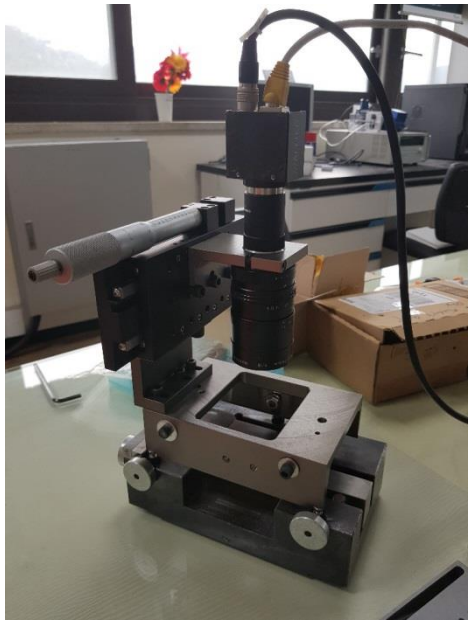

Figure 3.14. Imaging system for digital image correlation (DIC)

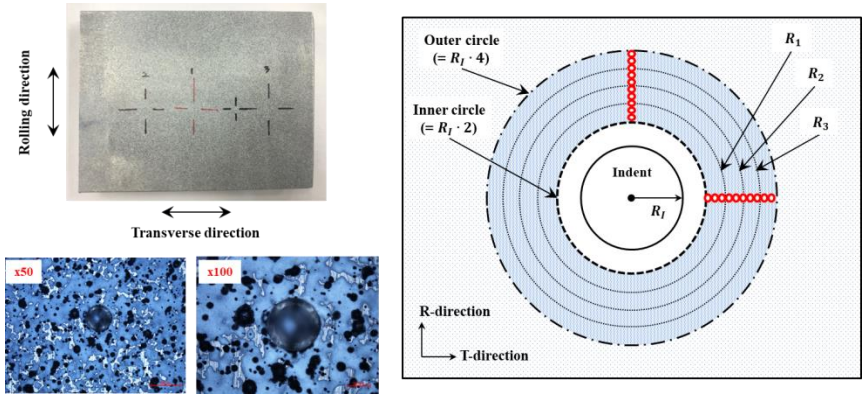

Figure 3.15. Analysis of surface displacement around spherical indentation for experimental verification

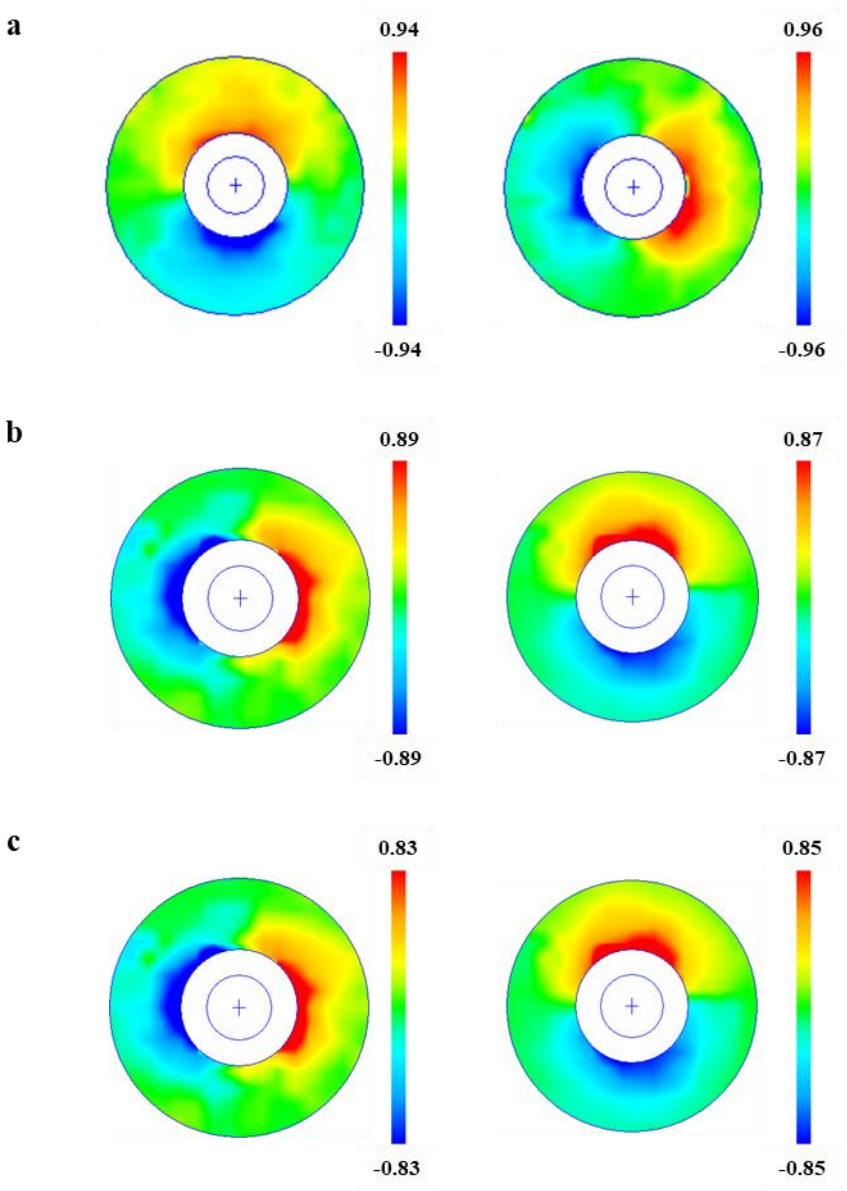

Figure 3.16. Results of surface displacement around spherical indentation for (a) as-received STS304L, (b) as-received S20C and (c) as-received STS410

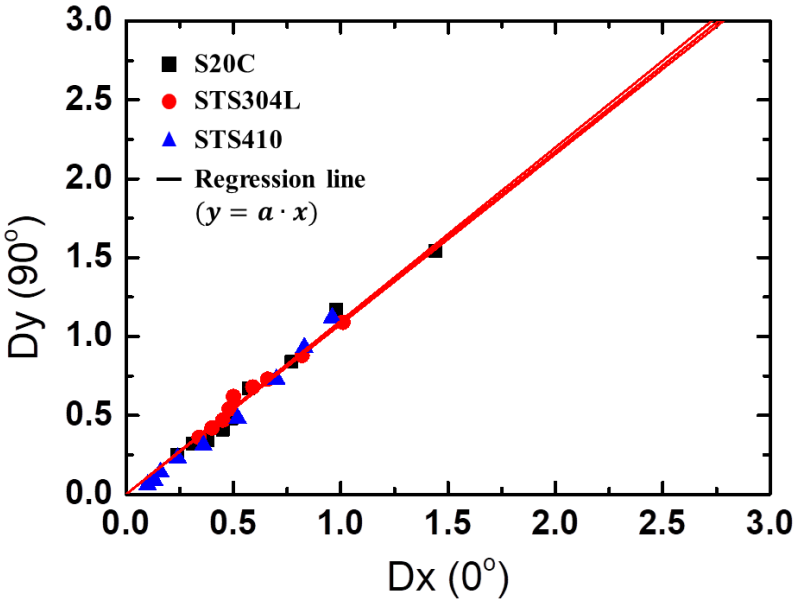

Figure 3.17. Linear line slope of surface displacement around spherical indentation for as-received STS304L, as-received S20C and as-received STS410

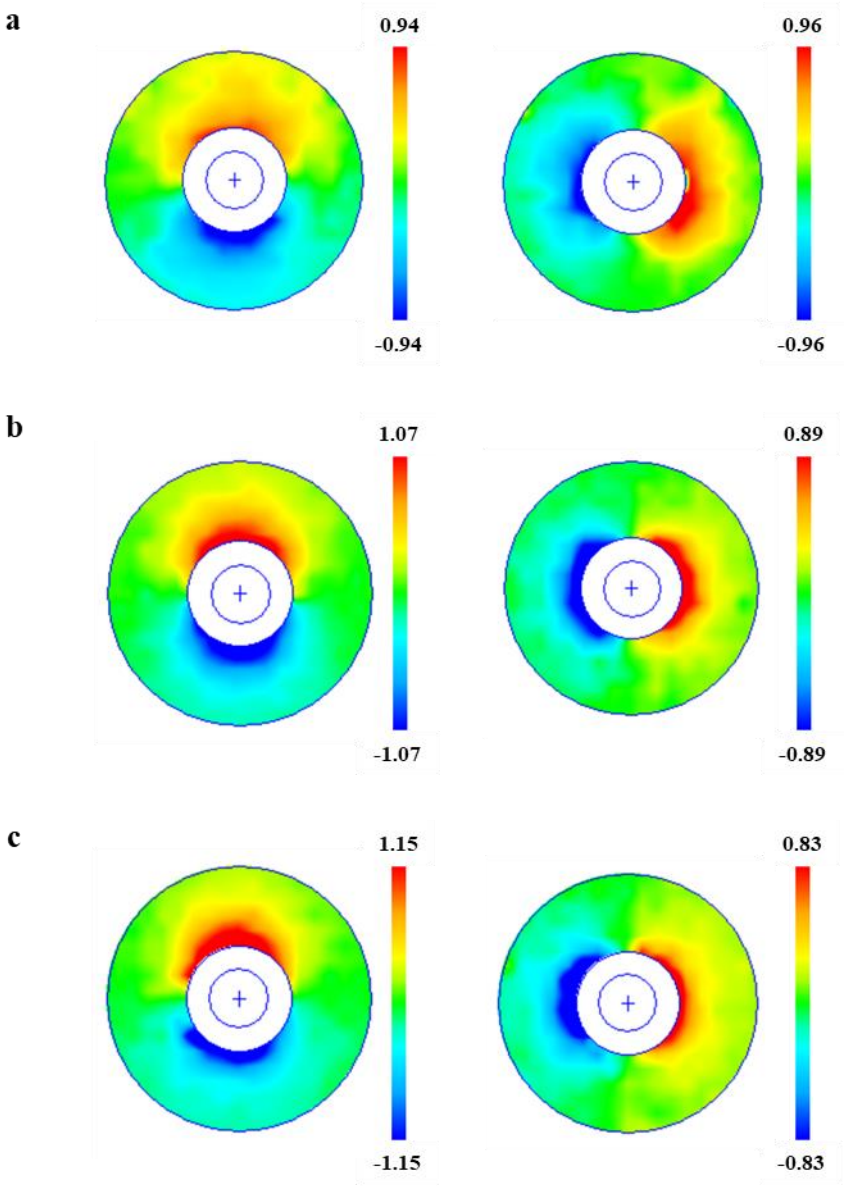

Figure 3.18. Results of surface displacement around spherical indentation for (a) as-received, (b) 10% cold rolled and (c) 20% cold rolled STS304L

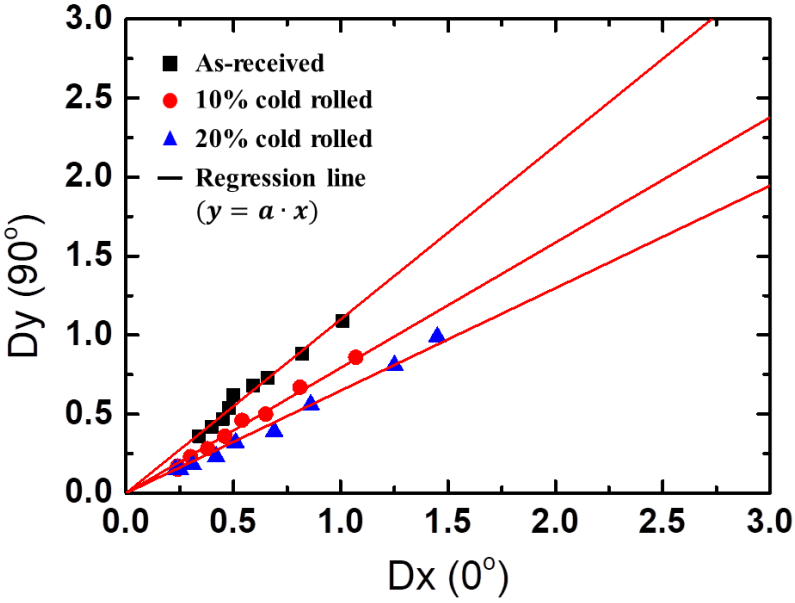

Figure 3.19. Linear line slope of surface displacement around spherical indentation for as-received, 10% cold rolled and 20% cold rolled STS304L

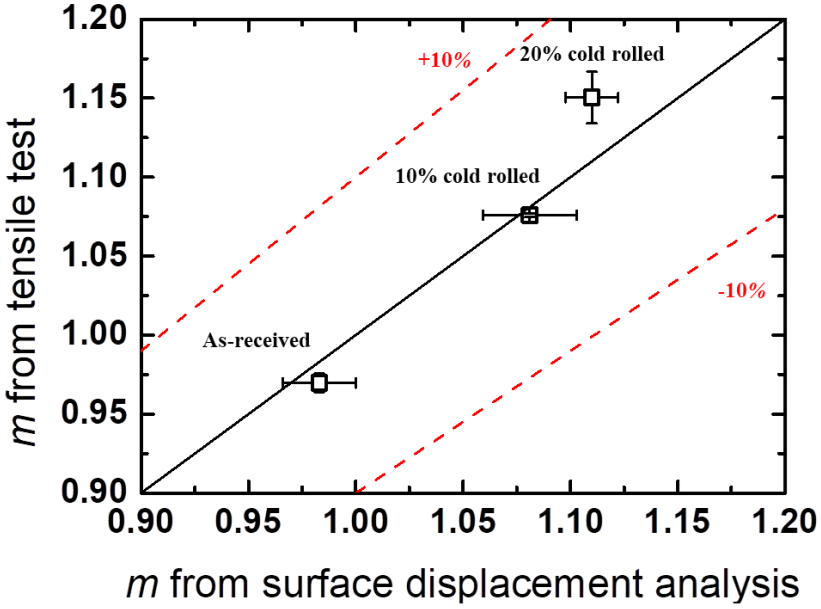

Figure 3.20. Comparison of estimated directional ratio of yield strength (*m*) and that of uniaxial tensile test for as-received, 10% cold rolled and 20% cold rolled STS304L

References

[1] E.c.-o.f. Accreditation, EA Guidelines on the estimation of uncertainty in hardness measurements, (2002).

[2] H. Lee, J. Haeng Lee, G.M. Pharr, A numerical approach to spherical indentation techniques for material property evaluation, Journal of the Mechanics and Physics of Solids 53(9) (2005) 2037-2069.

[3] T.-H. Pham, S.-E. Kim, Determination of equi-biaxial residual stress and plastic properties in structural steel using instrumented indentation, Materials Science and Engineering: A 688 (2017) 352-363.

[4] S.-K. Kang, Y.-C. Kim, K.-H. Kim, J.-Y. Kim, D. Kwon, Extended expanding cavity model for measurement of flow properties using instrumented spherical indentation, International Journal of Plasticity 49 (2013) 1-15.

[5] S.-H. Kim, M.-K. Baik, D. Kwon, Determination of precise indentation flow properties of metallic materials through analyzing contact characteristics beneath indenter, Journal of engineering materials and technology 127(3) (2005) 265-272.

[6] Y.-T. Cheng, C.-M. Cheng, Scaling, dimensional analysis, and indentation measurements, Materials Science and Engineering: R:

Reports 44(4) (2004) 91-149.

[7] S. Suresh, T.-G. Nieh, B. Choi, Nano-indentation of copper thin films on silicon substrates, Scripta Materialia 41(9) (1999) 951-957.

[8] A. Yonezu, K. Yoneda, H. Hirakata, M. Sakihara, K. Minoshima, A simple method to evaluate anisotropic plastic properties based on dimensionless function of single spherical indentation – Application to SiC whisker-reinforced aluminum alloy, Materials Science and Engineering: A 527(29) (2010) 7646-7657.

[9] A. Yonezu, Y. Kuwahara, K. Yoneda, H. Hirakata, K. Minoshima, Estimation of the anisotropic plastic property using single spherical indentation—An FEM study, Computational Materials Science 47(2) (2009) 611-619.

[10] K. Yoneda, A. Yonezu, H. Hirakata, K. Minoshima, Estimation of anisotropic plastic properties of engineering steels from spherical impressions, International Journal of Applied Mechanics 2(02) (2010) 355-379.

[11] S.M. Kalkhoran, Characterization of Anisotropic Plasticity in Material Systems Using ModifiedIndentation-Based Techniques, Northeastern University, 2013.

[12] T. Nakamura, Y. Gu, Identification of elastic–plastic anisotropic

parameters using instrumented indentation and inverse analysis, Mech. Mater. 39(4) (2007) 340-356.

[13] M. Wang, J. Wu, X. Zhan, R. Guo, Y. Hui, H. Fan, On the determination of the anisotropic plasticity of metal materials by using instrumented indentation, Materials & Design 111 (2016) 98-107.

Chapter 4

IMPROVEMENT OF EVALUATING INDENTATION YIELD STRENGTH

Contents

4.1. Motivation and Research Flow

Tabor [1] suggested an experimental relationship between flow stress and strain in uniaxial tension and such spherical indentation parameters as indentation load, contact radius and indenter radius. Following Tabor's approach, extensive work on evaluating tensile properties using the spherical indentation has been conducted. Ahn and Kwon [2] suggested a new definition of flow strain expressed by the shear strain at the contact edge beneath the spherical indenter and investigated the ratio of mean indentation pressure to flow stress in spherical indentation for power-law-hardening metals. Recently, Kang et al. [3], analyzing the stress field beneath a spherical indenter, found that the relation between mean indentation pressure and uniaxial flow stress depends on the material flow properties. In addition, they modified the relationship between yield strength and Brinell hardness (the so-called Meyer relation [4]) and showed good agreement between the indentation yield strength and the yield strength measured by uniaxial tensile testing. Although new research on evaluating tensile properties using the IIT continues, little work has been done on uncertainty estimation. Research on the

uncertainty in yield strength in particular is needed because the stress variation at the yield point is more severe than at the necking point, increasing the standard uncertainty [5].

According to ISO GUM [6], uncertainty is a parameter expressing doubt about the validity of a measurement result and characterizes the dispersion of a value that could reasonably be attributed to the measurand. Uncertainty is of two classes: Type A and Type B. Type A evaluation is defined as the method involving statistical analysis of experimental data and Type B evaluation is defined as the method based on scientific judgment of all information available on parameter variability except for experimental data. Type A and Type B uncertainty are important for test methods because they are indexes of reliability. Jeon et al. [5] suggested a simplified uncertainty estimation method for indentation tensile properties through measurands defined by a mathematical model. However, they only consider Type A uncertainty, and whether the final expanded uncertainty depends on indentation yield strength was not verified for metallic materials with various hardening behaviors. Moreover, so far the uncertainty difference in the yield strength as measured by the IIT and uniaxial tensile testing remains unclear and it is

still unknown how uncertainty sources quantitatively affect the uncertainty of indentation yield strength.

In this study, we use the modified Meyer relation [3] to propose a method for accurately estimating the uncertainty of indentation yield strength by taking into account Type A and Type B uncertainty. A relationship between the uncertainty and the indentation yield strength is demonstrated for metallic materials with various hardening behaviors. Using this method, we quantitatively compared the uncertainty level of the yield strength as evaluated by IIT and uniaxial tensile testing. To determine the dominant measurand affecting the final expanded uncertainty, the degree of contribution (DOC) and the coefficient of variation (CV) of each measurand were analyzed. Based on these results, we verify the effects of two major uncertainty sources influenced by surface contact: indentation sample surface roughness and angular misalignment between the surface normal of the sample and the symmetric axis of the indenter. The surface roughness was controlled using 400-, 1000- and 2000-grit paper and the misalignment angle ranged over 0 °, 1 ° and 2 °. From the relationships between the uncertainty and the major uncertainty sources, acceptable surface roughness and standard

uncertainty of the angular misalignment were proposed for which the IIT has uncertainty similar to that of uniaxial tensile testing.

4.1.1. Evaluation of indentation yield strength

Meyer [4] has shown that geometrically similar indentation gives the same Brinell hardness, now called the Meyer relation:

$$\frac{L}{d^2} = C \cdot \left(\frac{d}{D} \right)^{m-2} \tag{1}$$

where L is the indentation load, d is the residual diameter, D is the indenter diameter, C is the material constant and m is the Meyer index determined by fitting. Eq. (1) can be rewritten as a relation for the geometrical shape of the spherical indenter as:

$$P_m = \frac{4}{\pi} \cdot C \cdot \left(\frac{a}{R} \right)^{m\text{-}2} \tag{2}$$

where P_m is mean indentation pressure, a is contact radius and R is the radius of the spherical indenter. If we consider the constitutive Hollomon equation ($\sigma_t = K \cdot \varepsilon_t^n$, where σ_t, ε_t, K and n are flow stress, flow strain, strength coefficient and strain-hardening exponent in uniaxial tension) [3], the strain-hardening exponent n is given by

$$n = m - 2 \tag{3}$$

Therefore, Eq. (3) is substituted into Eq. (2) so that the material constant C in Eq. (2) can be rewritten as follows:

$$C = \frac{L}{4 \cdot a^2} \cdot \left(\frac{R}{a} \right)^n = \frac{L \cdot R^n}{4 \cdot a^{n+2}} \tag{4}$$

The contact radius is determined from the contact depth h_c and R from the geometrical contact morphology assuming a perfectly axisymmetric spherical indenter:

$$a = \sqrt{2Rh_c - h_c^2} \tag{5}$$

where h_c is obtained by the Oliver and Pharr [7] equation through a geometrical relationship:

$$h_c = h_{\max} - h_d \tag{6}$$

where $h_{\max}$ is the maximum depth and h_d is the deflection of the surface at the contact perimeter. Here h_d is determined by

$$h_d = \varepsilon \cdot \frac{L_{\max}}{S} \tag{7}$$

where ε is a geometrical constant (0.75 for a spherical indenter) and S is the stiffness determined by the initial slope of the unloading curve.

George et al. [8] found experimentally the following relationship between yield strength and the material constant:

$$\sigma_y = \beta \cdot C \tag{8}$$

where β is a constant depending on the material class; it is reported to be about 0.23 for steel [3].

Kang et al. [3] reanalyzed the Meyer relation [4] using the results of stress-field analysis and the constitutive equation and found that β is related to a combination of strain-hardening exponent, elastic modulus and plastic constraint factor. Using this result, they suggested a modified Meyer relation (Eq. (9)) and a quantitative relationship between a modified multiplying constant β' and the strain-hardening exponent (Eq. (10)):

$$\sigma_y = \beta' \cdot C^{\frac{1}{1-n}} \tag{9}$$

$$\beta' = f_{\beta'}(p) = -13.43 \cdot n^3 + 11.53 \cdot n^2 - 3.42 \cdot n + 0.36 \tag{10}$$

Because the strain-hardening exponent must be pre-determined in order to predict the yield strength using this modified Meyer relation, Kang et al. [3] proposed a quantitative relationship between the strain-hardening exponent and the ratio of loading slopes:

$$n = f_n(p) = -52.24 \cdot p^3 + 228.18 \cdot p^2 - 329.32 \cdot p + 157.31 \quad (11)$$

where p is the ratio of loading slopes at two fixed contact radii a_1 = 150 μm and a_2 = 200 μm in the indentation load and contact radius curve as shown in **Fig. 4.1 (b)**:

$$p = \left.\frac{dL}{da}\right|_{a_2} \Big/ \left.\frac{dL}{da}\right|_{a_1} \quad (12)$$

4.1.2. Possible uncertainty sources in indentation test

As shown in Table 4.1 and 4.2, the expanded uncertainties of indentation yield strength show larger and wider dispersion than that of uniaxial tensile testing. Diverse sources affect the uncertainty more or less seriously: test system (test sample, experimental equipment, etc.), environment, operator, etc [9]. We focused on the material-extrinsic uncertainty sources that can occur in the test system, not material-intrinsic uncertainty sources (e.g. grain-size heterogeneity). In addition, we assumed the uncertainty sources other than those of the test system are negligible because a single operator performed the IITs and the uniaxial tensile tests in the same laboratory.

For the test system, as the IIT evaluates local properties by mechanical contact between indenter and material surface, uncertainty sources influenced by the surface contact mainly affect the final uncertainty of the IIT, unlike in uniaxial tensile testing. One of the uncertainty sources influenced by the surface contact is sample surface roughness [10, 11]. This surface roughness cannot be completely eliminated, since no surface is perfectly flat, and this affects the

indentation load and depth curve. If the indenter is located on a peak, the material is deformed to a greater indentation depth at relatively low load; if it is located in a valley, the opposite is observed on a rough-surface sample at nano-scale. Thus, the indentation load and depth curves are scattered depending on whether indentation is conducted on a peak or in a valley [12]. Although surface roughness in micro-indentation is less influential than during nano-indentation, it remains nevertheless one of the sources affecting uncertainty of the IIT. In general, it is difficult to control acceptable surface roughness in the field, so the uncertainty level influenced by surface roughness must be verified.

4.2. Uncertainty of indentation yield strength

We base our uncertainty estimation of the indentation yield strength obtained from the modified Meyer relation on the ISO GUM [6] and the A2LA Guide [13]. The brief procedure for estimating uncertainty has four steps: step 1: set of the mathematical functions for the measurement; step 2: evaluation of the standard Type A and Type B uncertainties; step 3: determination of the combined uncertainties; step 4: determination of the expanded uncertainties. As shown in Fig. 4.1, measurands in this study are the experimental data directly obtained from the indentation load and depth curves and load and contact radius curves through repeated tests under the same conditions; their values and uncertainties are directly determined in the measurement. The sum of the uncertainties of all measurands affects the uncertainty of the final result. Therefore, to estimate the uncertainty of the indentation yield strength calculated from the modified Meyer relation, we created a mathematical function consisting of the parameters directly obtained from the indentation load and depth curve, not from a mathematical model.

4.2.1 Uncertainty evaluation method of indentation yield strength

In order to express Eq. (9) as the measurands (p , S , L and h), the material constant C is rewritten by substituting Eqs. (5), (6) and (7) into Eq. (4) as follows:

$$\begin{aligned} C &= f\left(p, S, L, h\right) \\ &= \frac{L \cdot R^{f_n(p)}}{4}\left[\left(2 \cdot R \cdot L\right)+\left(\frac{3 \cdot L \cdot \left(h-R\right)}{2 \cdot S}\right)-h^2-\left(\frac{9 \cdot L^2}{16 \cdot S^2}\right)\right]^{-\frac{f_n(p)}{2}-1} \end{aligned} \tag{13}$$

where $f_n(p)$ is the cubic function of the ratio of loading slope to determine the strain-hardening exponent (Eq. (11)). Finally, Eq. (9) can be expressed as the measurands by substituting Eqs. (10), (11) and (13) into Eq. (9) as follows:

$$\begin{aligned} \sigma_y &= f(p, S, L, h) \\ &= f_{\beta'}(p)\left[\frac{L \cdot R^{f_n(p)}}{4} \cdot \left[\left(2 \cdot R \cdot h\right)+\left(\frac{3 \cdot L \cdot \left(h-R\right)}{2 \cdot S}\right)-h^2-\left(\frac{9 \cdot L^2}{16 \cdot S^2}\right)\right]^{\frac{f_n(p)}{2}-1}\right]^{\frac{1}{1-f_n(p)}} \end{aligned} \tag{14}$$

where $f_{\beta'}(p)$ is the function of the ratio of loading slope to determine a modified multiplicative constant β' (Eq. (10)) given by substituting Eq. (11) into Eq. (10).

The evaluation of uncertainty is classified into Type A and Type B. Type A evaluation is defined as the method by the statistical analysis of experimental data, and Type B evaluation is defined as the method based on scientific judgment using all information available on parameter variability except the experimental data. Since all uncertainties must be converted to standard uncertainties and expressed at the same confidence level, both Type A and Type B uncertainties are expressed as standard uncertainties. Therefore, we estimated the Type A uncertainties of the ratio of loading slope and stiffness through repeated indentation tests and calculated the standard uncertainties $\left(u_{i,A}\right)$ using the following equations:

$$\bar{x} = \frac{1}{j}\sum_{i=1}^{j} x_i \tag{15}$$

$$u_{i,A} = \sqrt{\frac{1}{j}\sum_{i=1}^{j}\left(x_i - \bar{x}\right)^2} \tag{16}$$

where x_i is the repeatedly measured experimental data, $\bar{x}$ is the average value and j is the number of experiments. We then estimated the Type B uncertainties using the resolution of the load and depth sensor and calculated the standard uncertainties $\left(u_{i,B}\right)$ using the rectangle distribution:

$$u_{i,B} = \frac{r}{\sqrt{3}} \tag{17}$$

where r is the resolution of the load and depth sensor.

In order to combine the uncertainties, their units must be the same. So, the standard uncertainties of Type A and Type B are combined by a root-sum-square method and this result is defined as the combined standard uncertainty. The coefficients of sensitivity $\left(c_p, c_S, c_L, c_h\right)$, which are a type of weighting values, were calculated using Eq.(14) as:

$$c_p = \frac{\partial \sigma_y}{\partial p}, \quad c_S = \frac{\partial \sigma_y}{\partial S}, \quad c_L = \frac{\partial \sigma_y}{\partial L} \quad and \quad c_h = \frac{\partial \sigma_y}{\partial h} \tag{18}$$

Using Eqs. (15), (16), (17) and (18), we estimated the combined standard uncertainty $\left(u_c\right)$ as:

$$u_c^2 = \sum_i^N \left(\frac{\partial f}{\partial x_i} \right)^2 \cdot u_i^2 = c_p^2 \cdot u_p^2 + c_S^2 \cdot u_S^2 + c_L^2 \cdot u_L^2 + c_h^2 \cdot u_h^2 \tag{19}$$

Eq. (19) is valid if two or more measurands are independent [6]. The measurands used in Eq. (19) can be considered independent because they are not chemical but physical measurands [5]. To estimate the coverage factor $\left(k\right)$, the confidence level of the standard uncertainty must be considered. In general, k is adopted at a 95.45% confidence level and the effective degree of freedom $\left(v_{eff}\right)$ is determined by the Welch-Satterthwaite formula. Thus, the k value was determined using

Student's *t*-table:

$$\nu_{eff} = \frac{u_c^4(y)}{\sum_{i=1}^{N} \frac{\left[c_i u(x_i)\right]^4}{\nu_i}} \tag{20}$$

where ν_i is the degrees of freedom. Finally, the expanded uncertainty $\left(U_{\sigma_y}\right)$ was estimated using Eq. (21) and expressed as the relative percent value normalized by the indentation yield strength as shown in Eq. (22):

$$U_{\sigma_y} = k \cdot u_c \tag{21}$$

$$U_{\sigma_y}(\%) = \frac{U_{\sigma_y}}{\sigma_y} \times 100 \tag{22}$$

The uncertainties were calculated following the flow chart in Fig. 4.2.

4.2.2 Uncertainty of indentation test and uniaxial tensile test

Figure 4.3 shows five indentation load and depth curves obtained under the same test conditions using the same AIS 3000 equipment for carbon steel SKD11 and copper alloy C10200 among eighteen metallic materials. Their yield strengths as obtained from uniaxial tensile tests are 413.30 MPa and 212.20 MPa, respectively. Using these indentation load and depth curves, the indentation yield strength was determined by the modified Meyer relation (Eq. (9)) and the expanded uncertainty of the indentation yield strength was calculated considering Type A and Type B uncertainty in Sec. 4.2.1. Table 4.1 shows the standard uncertainties, degree of freedom, k and the expanded uncertainties for the indentation yield strength for the 18 metallic materials. The expanded uncertainties of the indentation yield strength range from 2.12% to 18.69%, with average value 10.46% and standard deviation 5.54%.

As described in Eq. (22), the final expanded uncertainties are the relative percent values influenced by the average values of the yield strength. Therefore, we must demonstrate whether the expanded uncertainty is dependent on the indentation yield strength or not. Figure 4.4 (a) shows the relationship between the expanded uncertainty and the

indentation yield strength. These expanded uncertainties have a negative relationship with the indentation yield strength with polynomial regression line with slope 0.01×10^{-1}, and the p-value is evaluated at 0.93. We see from this result that there is no correlation between the expanded uncertainty expressed as relative value and the indentation yield strength because the p-value is much greater than 0.05 with a 95% confidence level [15]. Therefore, the expanded uncertainties estimated in this study are influenced not by yield strength but by uncertainty sources.

The uncertainty of the uniaxial tensile testing was estimated using the example in A2LA [13]. The mathematical function of yield strength is:

$$\sigma_y = f\left(L,T,W\right) = \frac{L}{T \cdot W} \tag{23}$$

where L is the load at the 0.2 offset yield point in the stress and strain curve, T is the thickness and W is the width of the rectangular tensile sample. The uncertainty of the yield strength was calculated based on Sec. 4.2.1. Table 4.2 presents the standard uncertainties, degree of freedom, k and the expanded uncertainties for the yield strength obtained from

the uniaxial tensile test. The expanded uncertainties of the yield strength range from 0.92% to 12.60%, with average value 5.08% and standard deviation 3.36%. The expanded uncertainties of the indentation yield strength present a larger and wider dispersion than that of the uniaxial tensile testing. This means that the IIT system can be affected by uncertainty sources different from the uniaxial tensile testing.

4.3. Effect of uncertainty sources on uncertainty of indentation yield strength

The measurands obtained directly from the experiment affect the final uncertainty of the mathematical function. So, if the dominant measurand can be determined, the uncertainty of the mathematical function can be controlled. The degree of contribution (DOC) [14] was calculated to analyze quantitatively the contribution of the measurands to the expanded uncertainty. The DOC of measurands is defined as:

$$DOC(\%) = \frac{c_i^2 u_i^2}{u_c^2} \times 100 \tag{24}$$

The $DOCs$ of the measurands to the expanded uncertainty are shown in Table 4.3. The $DOCs$ of the ratio of loading slope are about 99% for all eighteen metallic materials, the largest among the measurands. On the other hand, the $DOCs$ of stiffness, load and depth are all less than 1%. Therefore, the expanded uncertainty of indentation yield

strength is dominated by the ratio of loading slope.

In addition to DOC, we introduce a coefficient of variation (CV) [14] as another statistic to confirm that the expanded uncertainty of indentation yield strength is dominated by the variation in the ratio of loading slope. The CV is a value that can be used to compare distributions of groups when the difference in the average values of groups is very large due to different units. The CV of the population is defined as:

$$CV(\%) = \frac{u_i}{\bar{x}} \times 100 \tag{25}$$

Figure 4.4 (b) presents the relationship between CV of measurands and the expanded uncertainty. The CVs of the ratio of loading slope and the expanded uncertainties are positively correlated with the polynomial regression line with slope 3.13, and the p-value is evaluated at 0.01×10^{-6}. The CVs of the stiffness and the expanded uncertainties are positively correlated with polynomial regression line with slope 0.38, but

these data points are scattered around the polynomial regression line. The CVs of the indentation load and the CVs of the indentation depth were about 0.01 and 0.04, respectively. They were almost the same for all materials because the indentation load and depth were evaluated as Type B uncertainty. Thus, the CV of the ratio of loading slope is more strongly correlated with the expanded uncertainty than the CVs of other measurands. This means that the standard uncertainty and the expanded uncertainty of the indentation yield strength are dominated by the variation in the ratio of loading slope, as with the DOC results. This result can be qualitatively understood from the uncertainty function (Eq. (14)), which contains an exponential term of the ratio of loading slope. Thus, if the uncertainty sources causing the slope variation in the indentation loading curve are controlled, the uncertainty of indentation yield strength can be significantly reduced.

As shown in Table 4.1 and 4.2, the expanded uncertainties of indentation yield strength show larger and wider dispersion than that of uniaxial tensile testing. Diverse sources affect the uncertainty more or less seriously: test system (test sample, experimental equipment, etc.), environment, operator, etc [9]. We focused on the material-extrinsic

uncertainty sources that can occur in the test system, not material-intrinsic uncertainty sources (e.g. grain-size heterogeneity). In addition, we assumed the uncertainty sources other than those of the test system are negligible because a single operator performed the IITs and the uniaxial tensile tests in the same laboratory. For the test system, as the IIT evaluates local properties by mechanical contact between indenter and material surface, uncertainty sources influenced by the surface contact mainly affect the final uncertainty of the IIT, unlike in uniaxial tensile testing. One of the uncertainty sources influenced by the surface contact is sample surface roughness [10, 11]. This surface roughness cannot be completely eliminated, since no surface is perfectly flat, and this affects the indentation load and depth curve. If the indenter is located on a peak, the material is deformed to a greater indentation depth at relatively low load; if it is located in a valley, the opposite is observed on a rough-surface sample at nano-scale. Thus, the indentation load and depth curves are scattered depending on whether indentation is conducted on a peak or in a valley [12]. Although surface roughness in micro-indentation is less influential than during nano-indentation, it remains nevertheless one of the sources affecting uncertainty of the IIT. In general, it is difficult to control acceptable surface roughness in the field, so the uncertainty level

influenced by surface roughness must be verified.

A standard hardness block with 200 HV 10 was chosen as the reference material to verify the effect of surface roughness. We controlled the surface roughness using 400-, 1000- and 2000-grit paper on the as-received hardness block, which was manufactured through polishing and wet buffing. IITs were performed for the four types of surface roughness, the indentation load and depth curves for which are presented in Fig. 4.5 (a). The indentation yield strength and expanded uncertainty were then calculated based on Sec. 4.2. Figure 4.6 (a) shows the effect of the expanded uncertainty depending on the surface roughness R_a for the standard-hardness block with 200 HV 10 and nine metallic materials. The expanded uncertainty and R_a are positively correlated with the polynomial regression line with slope 0.24, and the p-value is evaluated at 0.03×10^{-3}. For the hardness block polished with 400-grit paper, the expanded uncertainty is about 17.71%, almost double that of the hardness block polished with 1000-grit paper. For the hardness block polished with 1000-grit paper, the expanded uncertainty is about 10.49%, similar to the hardness block polished with 2000-grit paper. For the hardness block polished with 2000-grit paper, R_a is about 13.53 nm and the expanded

uncertainty is about 8.38%, a significant 6.26-fold increase over the as-received hardness block (for which R_a is about 4.01 nm and the expanded uncertainty is about 1.34%). This result can be simply explained. The change in the standard uncertainty of the ratio of loading slope depending on R_a. R_a of about 13.53 nm, 55.95 nm and 71.25 nm leads to a slight 0.99-, 0.97- and 0.98-fold decrease, respectively, in the average of the ratio of loading slope, but leads to a significant 6.29-, 7.67- and 12.58-fold increase, respectively, in the standard uncertainty of the ratio of loading slope compared to R_a 4.01 nm. Thus, this significantly increased standard uncertainty of the ratio of loading slope increases the final expanded uncertainty of the indentation yield strength.

The metallic materials in Fig. 4.6 (a) were selected for each of three materials in ranges of uncertainty differences between the IIT and the uniaxial tensile tests of less than about 3%, from about 3% to about 5%, and more than about 7%, as shown in Table 4.1. These metallic materials polished with 2000-grit paper have difference values of R_a and their expanded uncertainty increases linearly depending on increasing R_a, as in the results of the hardness block. From this result, we analyzed the

trend of expanded uncertainty differences between IIT and uniaxial tensile testing $(U_{\sigma_y^{IIT}}(\%) - U_{\sigma_y^{Tension}}(\%))$ depending on R_a to confirm whether surface roughness is an uncertainty source that makes the uncertainty of IIT larger than that of uniaxial tensile testing. The metallic materials with larger expanded uncertainty of IIT than that of uniaxial tensile testing are presented in Fig. 4.6 (b); we see that the expanded uncertainty differences between IIT and uniaxial tensile testing are proportional to R_a, and the p-value is evaluated at 0.02×10^{-1}. Therefore, surface roughness is one of the uncertainty sources that make the uncertainty of IIT larger than that of uniaxial tensile testing. Considering the same uncertainty of IIT and uniaxial tensile testing, we recommend an R_a of about 18 nm or less for indentation samples, as determined by the linear regression analysis function $\left(y = -6.03 + 0.33 \cdot x\right)$ obtained from the relationship between the expanded uncertainty difference and R_a.

In addition to the effect of surface roughness, another issue affecting the uncertainty of the IIT is the angular misalignment between the surface normal of the sample and the symmetric axis of the indenter [11]. Due to

the structural tolerance of the experimental equipment and the sample imperfection caused by mechanical polishing, the sample surface cannot be perfectly perpendicular to the indenter. Angular misalignment causes incomplete contact between the indenter and material surfaces that degrades the accuracy and reproducibility of the indentation load and depth curves [15]. Thus, we explored the effect of angular misalignment on the uncertainty of indentation yield strength. To control the angular misalignment between the surface normal of the sample and the symmetric axis of the indenter, the angle of the sample was adjusted with the indenter's angle fixed. The IITs were performed four times per misalignment angle over 0 °, 1 ° and 2 ° for an as-received standard hardness block with 200 HV 10, the indentation load and depth curves for which are presented in Fig. 4.5 (b). The indentation yield strength and the expanded uncertainty were then estimated for combinations of four indentation load and depth curves with the same standard uncertainty of misalignment angles. The effect of angular misalignment on expanded uncertainty of indentation yield strength is shown in Fig. 4.7. When the four IITs with the same angle 0 ° were carried out, the expanded uncertainty was about 1.34%. For the range from about 0.4 ° to 0.5 ° of standard uncertainty of misalignment angle, the maximum expanded

uncertainty is 8.42%. For the range from about 0.7 ° to 1.0 ° of standard uncertainty of misalignment angle, the maximum expanded uncertainty is 27.81%. This result can be clarified by the change in the ratio of loading slope depending on angular misalignment. Misalignment angles of 1 ° and 2 ° lead to a slight 1.02- and 1.09-fold increase, respectively, in the average of the ratio of loading slope, but lead to a significant 7.24- and 13.02-fold increase, respectively, in the standard uncertainty of the ratio of loading slope compared to 0 °. Therefore, if the surface of the sample is not perfectly perpendicular to the indenter, irregular ratios of loading slope will be evaluated in each IIT, which increases the uncertainty of indentation yield strength determined from combination of irregular loading slope ratios. From the linear regression analysis function $\left(y = -1.48 + 29.99 \cdot x\right)$ obtained from the relationship between the expanded uncertainty and the standard uncertainty of misalignment angle, when the standard uncertainty of the misalignment angle is under about 0.22 °, it is expected that the expanded uncertainty of IIT is similar to an average expanded uncertainty of 5.08% in the uniaxial tensile testing statistically analyzed here.

4.4. Issues and limitations

We propose a method for accurately estimating the uncertainty of indentation yield strength determined from the modified Meyer relation as a mathematical function of the measurement, taking into account Type A and Type B uncertainty based on the ISO GUM and the A2LA guide. The expanded uncertainties of the indentation yield strength for the 18 metallic materials studied range from 2.12% to 18.69%, with average value 10.46% and standard deviation 5.54%, which is wider and larger than that of the uniaxial tensile testing. The expanded uncertainty of the indentation yield strength increases with increasing surface roughness parameter, R_a and increasing standard uncertainty of misalignment angle. It is recommended that the acceptable surface roughness and standard uncertainty of misalignment angle must be below about 18 nm and 0.22 °, respectively, for the IIT to have uncertainty similar to uniaxial tensile testing.

However, in actual indentation tests, there may be various uncertainty sources besides surface roughness and misalignment angle. For example, the material-intrinsic sources were not considered in this study, but the

heterogeneity of material properties could also be a uncertainty source, which should also be considered in the evaluation of uncertainty. In addition, in order to compare the uncertainty of the indentation test with the uncertainty of the uniaxial tensile test, the uncertainty source that can occur in the uniaxial tensile test should be considered to provide a accurate uncertainty criterion for the indentation test. In another aspect, this study independently evaluated the influence of surface roughness and misalignment angle, which are sources of uncertainty, on final expanded uncertainty. However, in order to provide a criterion of acceptable uncertainty in indentation test, the effect of these two sources together on the final expanded uncertainty should be studied.

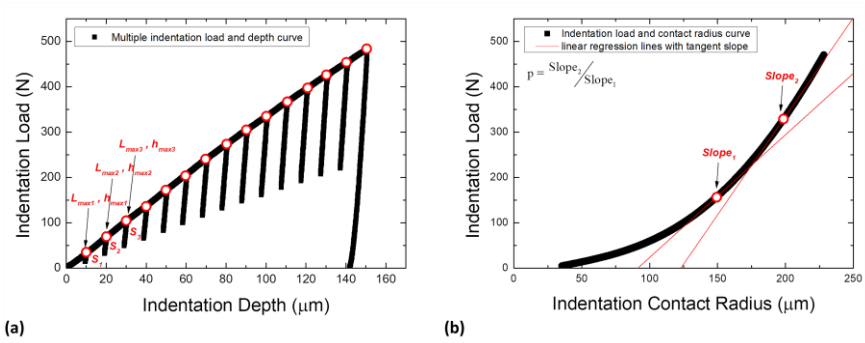

Figure 4.1. Measurands determined from (a) multiple indentation load and depth curve (b) indentation load and contact radius curve

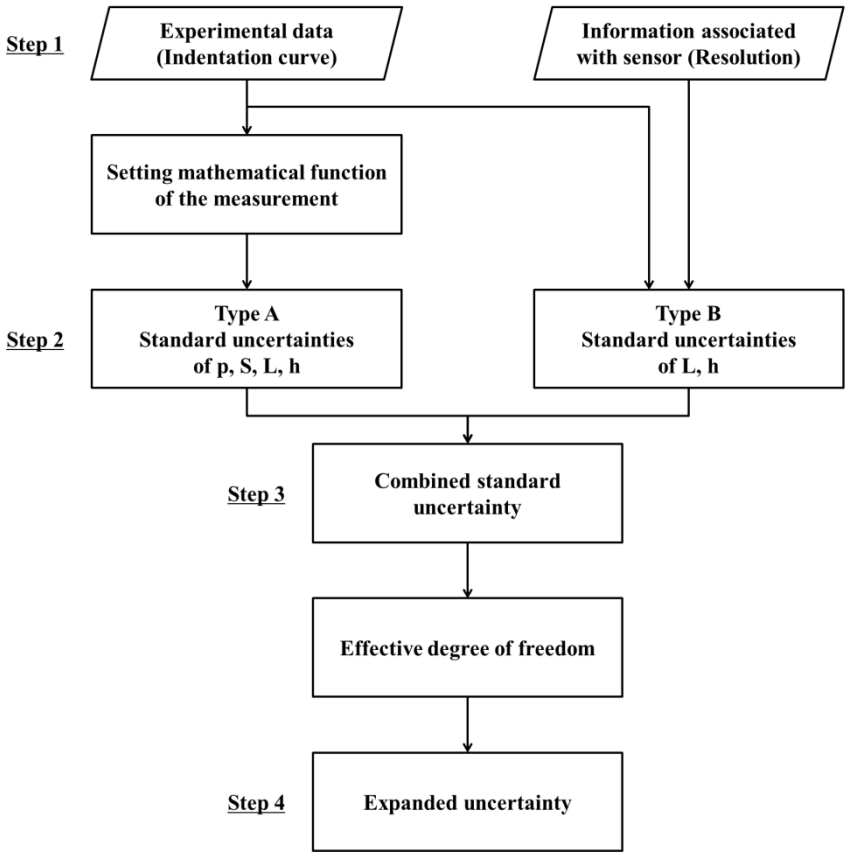

Figure 4.2. Schematic flow chart for estimating uncertainty of indentation yield strength

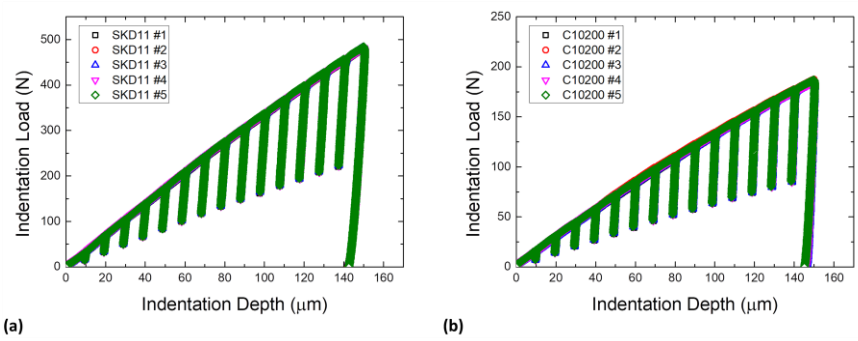

Figure 4.3. Five indentation load and depth curves for (a) SKD11 and (b) C10200 from AIS 3000 model

Table 4.1. Uncertainty table for the indentation yield strength

Materials	Standard uncertainties						U_{σ_y} (%)
	p	S $(N/\mu m)$	L (N)	h (μm)	v_{eff}	k	
SCM415	0.010	1.623			4.000		17.889
SKD11	0.002	0.806			4.001		2.662
SKD61	0.003	4.504			4.004		5.442
SKH51	0.004	3.982			4.003		6.029
SKS3	0.001	1.349			4.004		2.124
S20C	0.006	10.723			4.002		10.615
Al2024	0.012	1.395			4.000		18.694
Al7075	0.002	1.048			4.005		2.905
C10200	0.006	0.529			4.000		9.796
Ti-6Al-4V	0.010	0.753	0.032	0.058	4.000	2.870	15.949
STS303	0.012	7.857			4.000		16.746
STS316	0.006	5.256			4.000		9.719
STS316L	0.013	4.671			4.000		17.631
STS321	0.005	3.259			4.001		6.775
STS347	0.012	3.932			4.000		17.136
STS410	0.004	1.987			4.000		6.326
STS420J2	0.007	6.583			4.001		11.091
STS440C	0.007	7.085			4.003		10.817

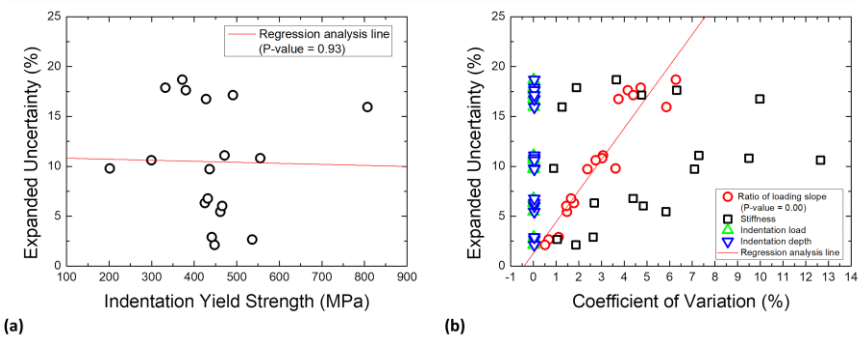

Figure 4.4. Regression analysis of expanded uncertainty with (a) indentation yield strength (b) coefficient of variation for measurands

Table 4.2. Uncertainty table for the yield strength obtained from uniaxial tensile testing

Materials	Standard uncertainties			v_{eff}	k	U_{σ_y}
	L (N)	T (mm)	W (mm)			$(\%)$
SCM415	396.077	0.013	0.007	4.030	2.870	11.875
SKD11	176.440	0.021	0.012	4.717	2.650	3.741
SKD61	45.074	0.013	0.007	8.831	2.320	0.917
SKH51	104.320	0.013	0.015	5.409	2.650	2.286
SKS3	254.519	0.010	0.006	4.117	2.870	4.792
S20C	279.669	0.010	0.008	4.044	2.870	8.381
Al2024	161.294	0.008	0.010	4.309	2.870	3.227
Al7075	118.956	0.006	0.014	5.277	2.520	1.698
C10200	334.388	0.008	0.010	4.019	2.870	12.597
Ti-6Al-4V	240.841	0.010	0.014	5.024	2.520	2.133
STS303	138.414	0.013	0.010	4.324	2.870	4.066
STS316	71.605	0.005	0.010	4.506	2.650	1.990
STS316L	91.488	0.006	0.005	4.129	2.870	3.040
STS321	250.887	0.013	0.007	4.120	2.870	5.959
STS347	144.589	0.007	0.006	4.281	2.870	2.859
STS410	434.319	0.007	0.010	4.039	2.870	8.169
STS420J2	240.711	0.015	0.004	4.136	2.870	5.641
STS440C	285.062	0.010	0.005	4.036	2.870	8.139

Table 4.3. Degree of contribution of measurands on expanded uncertainty of indentation yield strength

Materials	$p\ (\%)$	$S\ (\%)$	$L_{\max}\ (\%)$	$h_{\max}\ (\%)$
SCM415	99.996	0.002	0.000	0.002
SKD11	99.795	0.104	0.004	0.096
SKD61	99.491	0.486	0.001	0.022
SKH51	99.679	0.302	0.001	0.018
SKS3	99.417	0.427	0.009	0.147
S20C	99.760	0.233	0.001	0.006
Al2024	99.971	0.027	0.000	0.002
Al7075	99.203	0.720	0.008	0.069
C10200	99.991	0.001	0.003	0.005
Ti-6Al-4V	99.989	0.008	0.000	0.002
STS303	99.873	0.125	0.000	0.002
STS316	99.740	0.252	0.000	0.007
STS316L	99.965	0.034	0.000	0.001
STS321	99.843	0.146	0.001	0.011
STS347	99.973	0.026	0.000	0.002
STS410	99.914	0.068	0.001	0.016
STS420J2	99.873	0.122	0.000	0.005
STS440C	99.545	0.450	0.000	0.005

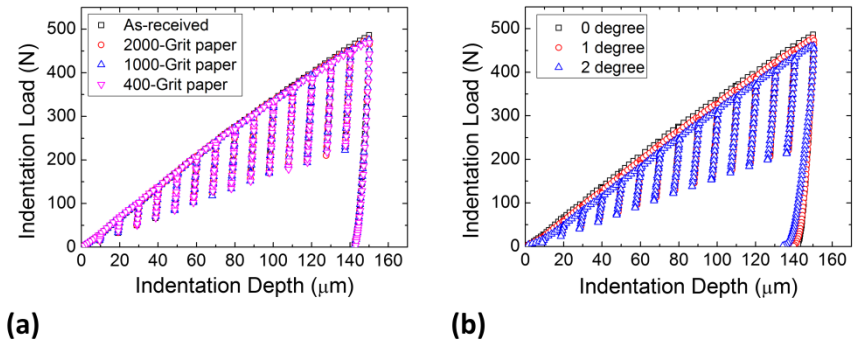

(a) **(b)**

Figure 4.5. Effect of (a) surface roughness and (b) angular misalignment on indentation load and depth curve for standard block with 200 HV 10

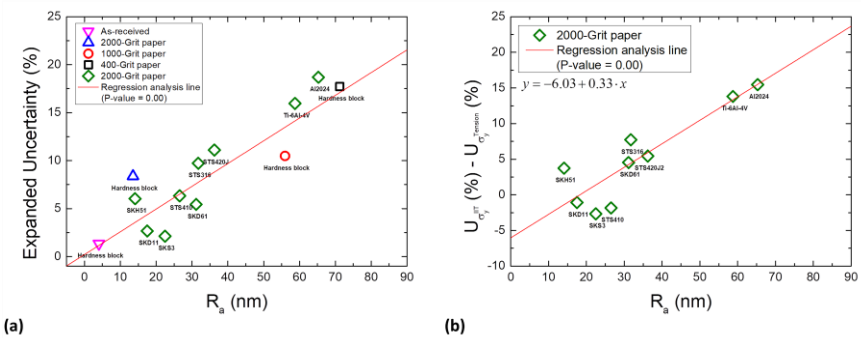

Figure 4.6. Effects of surface roughness on (a) expanded uncertainty of indentation yield strength and (b) difference between expanded uncertainty of IIT and uniaxial tensile testing for standard block with 200 HV 10 and metallic materials

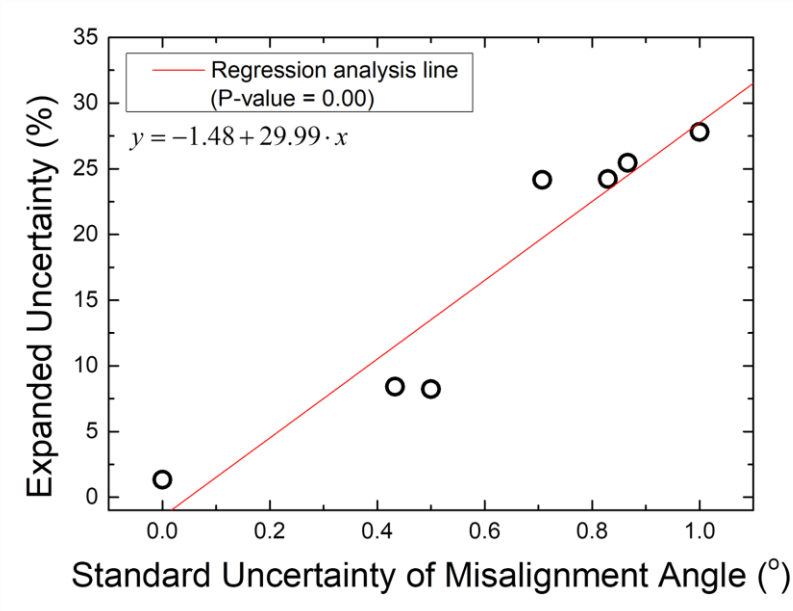

Figure 4.7. Effect of angular misalignment on expanded uncertainty of indentation yield strength for standard block with 200 HV 10

References

[1] D. Tabor, The hardness of metals, Clarendon, Oxford, 1951.

[2] J.-H. Ahn, D. Kwon, Derivation of plastic stress–strain relationship from ball indentations: Examination of strain definition and pileup effect, 2001.

[3] S.-K. Kang, Y.-C. Kim, K.-H. Kim, J.-Y. Kim, D. Kwon, Extended expanding cavity model for measurement of flow properties using instrumented spherical indentation, International Journal of Plasticity 49 (2013) 1-15.

[4] E. Meyer, Investigations of hardness testing and hardness, Phy. Z. 9 (1908) 66-74.

[5] E.-c. Jeon, J.-S. Park, D.-S. Choi, K.-H. Kim, D. Kwon, A Method for Estimating Uncertainty of Indentation Tensile Properties in Instrumented Indentation Test, 2009.

[6] ISO, Uncertainty of measurement - Part 3 : Guide to the expression of uncertainty in measurement(GUM:1995), ISO/IEC GUIDE 98-1:2009(E) (2008).

[7] W.C. Oliver, G.M. Pharr, An improved technique for determining hardness and elastic modulus using load and displacement sensing

indentation experiments, Journal of materials research 7(6) (1992) 1564-1583.

[8] R. A. George, S. Dinda, A. S. Kasper, Estimating yield strength from hardness data, 1976.

[9] S. Adamczak, J. Bochnia, B. Kaczmarska, Estimating the Uncertainty of Tensile Strength Measurement for A Photocured Material Produced by Additive Manufacturing, 2014.

[10] A. E2546-15, Standard Practice for Instrumented Indentation Testing, ASTM International (2015).

[11] G.E. Dieter, D.J. Bacon, Mechanical metallurgy, McGraw-hill New York1986.

[12] Y. Xia, M. Bigerelle, J. Marteau, P.E. Mazeran, S. Bouvier, A. Iost, Effect of surface roughness in the determination of the mechanical properties of material using nanoindentation test, Scanning: The Journal of Scanning Microscopies 36(1) (2014) 134-149.

[13] T.M. Adams, A2LA Guide for the estimation of measurement uncertainty in testing, (2002).

[14] C.J. Chieh, "Linear Regression: Making Sence of a Six Sigma Tool", iSixSigma Europe, https://www.isixsigma.com/tools-templates/regression/linear-regression-making-sense-six-sigma-tool/ (2008).

[15] N.B. Shahjahan, Z. Hu, Effects of angular misalignment on material property characterization by nanoindentation with a cylindrical flat-tip indenter, Journal of Materials Research 32(8) (2017) 1456-1465.

Chapter 5

CONCLUSION

5.1. Evaluation of indentation yield strength for anisotropic materials

We tried to obtain information on the directionality of yield strength from the surface deformation. The surface deformation can be measured by a strain gauge, which is widely used in uniaxial tensile or compression testing; however, the strain gauge has the limitation that only one strain value can be measured by one strain gauge. We chose the digital image correlation method here because its results can be analyzed from macro- to nanoscale, an attractive feature to combine with indentation's advantage of multi-scale testing. Therefore, in this study, we evaluated surface indentation displacement around the residual imprint using the digital image correlation method. After obtaining images of the testing area before and after indentation using the DIC imaging system (Fig. 3.2), displacements by indentation around the residual imprint can be evaluated by comparing the two images. 3D digital image correlation also lets us evaluate indentation pileup/sink-in; however, 2D digital image correlation was used here only to evaluate displacements parallel to the surface for convenience in testing.

First, the relationship between F/Eh^2 and m was confirmed by changing the yield strength of x-axis and the strain-hardening exponent for a fixed elastic modulus. The dimensionless terms F/Eh^2 and m have a linear relationship. As the yield strength of x-axis and strain-hardening exponent increased, the slope (α) and intercept (β) of the fitted line between F/Eh^2 and m increased. We obtained the linear function of $F/Eh^2 = f(m)$ for each σ_{Yx}/E and n.

Second, to reflect the yield strength of x-axis in the dimensionless function, the relationship between α, β and σ_{Yx}/E was confirmed for each imaginary materials. Finally, we obtained the following simple function formula for each strain-hardening exponent.

$$\frac{F}{Eh^2} = \left(a_1 \cdot \frac{\sigma_{Yx}}{E} + a_2\right) \cdot m + \left(b_1 \cdot \frac{\sigma_{Yx}}{E} + b_2\right)$$

$$\sigma_{Yx} = \left(\left(\frac{F}{Eh^2} - a_2 \cdot m - b_2\right) \cdot \frac{1}{a_1 \cdot m - b_1}\right) \cdot E$$

The spherical indentation loading curve obtained from FEA simulation was used to verifying the suggested equation by dimensional

analysis. We confirmed the relative error between the input yield strength of the x-axis and the yield strength of the x-axis calculated from the proposed model. It can be confirmed that the estimated results match well within 10% of the relative error. Therefore, this indentation model suggested in this study seems to have a good combination of indentation parameters and mechanical properties.

In the next step, the evaluation method for *m* in the proposed model was discussed. We assumed that the further away from the spherical indentation, the deformation decreases and becomes zero. Therefore, we fitted the linear lines of D_x and D_y past the origin. From this approach, it can be seen that as the directional ratio of yield strength increases, the slope of the linear line of D_x and D_y decreases. It also can be seen that as the directional ratio of yield strength increases, the slope of the linear line of D_x and D_y decreases. Using this phenomenon, we performed modeling to evaluate the directional ratio of yield strength.

The relationship between the linear line slope (*a*) of D_x and D_y and the directional ratio of yield strength was confirmed depending on the yield strength of x-axis and strain-hardening exponent. It can be

seen that the slope *a* is independent of yield strength of x-axis and strain-hardening exponent. Therefore, the following phenomenological model can be derived.

$$a = 1.00 \cdot m\left(= \frac{\sigma_{Yy}}{\sigma_{Yx}} \right)^{-3.05}$$

In order to verify the proposed method, As-received STS304L, 10% cold rolled STS304L, 20% cold rolled STS304L, as-received S20C and STS410 samples were prepared. It can be seen that the displacement in the direction with larger yield strength occurs less. From the DIC results, we measured the displacement slope *a* of x- and y-axis. For as-received samples, we can see that the displacement slope *a* is close to 1. On the other hand, we can confirm that the displacement slope *a* decreases as the cold rolling rate increases. Using the proposed model of directional ratio and surface displacement results, directional ratio of yield strength was estimated and compared to directional ratio obtained from the uniaxial tensile test. From this result, it can be confirmed that the proposed model shows good agreement.

5.2. Improvement of evaluating indentation yield strength

We propose a method for accurately estimating the uncertainty of indentation yield strength determined from the modified Meyer relation as a mathematical function of the measurement, taking into account Type A and Type B uncertainty based on the ISO GUM and the A2LA guide. The expanded uncertainties of the indentation yield strength for the 18 metallic materials studied range from 2.12% to 18.69%, with average value 10.46% and standard deviation 5.54%, which is wider and larger than that of the uniaxial tensile testing. The expanded uncertainties estimated here are influenced not by the indentation yield strength but by uncertainty sources because the p-value at 95% confidence level is much greater than 0.05. The $DOCs$ of the ratio of loading slope is about 99% for all 18 metallic materials, and the CVs of the ratio of loading slope are most strongly correlated with the expanded uncertainties among measurands. Thus, we concluded that the expanded uncertainty of indentation yield strength is dominated by the ratio of loading slope. The expanded uncertainty of the indentation yield strength increases with increasing surface roughness parameter, R_a and increasing standard

uncertainty of misalignment angle. It is recommended that the acceptable surface roughness and standard uncertainty of misalignment angle must be below about 18 nm and 0.22 °, respectively, for the IIT to have uncertainty similar to uniaxial tensile testing.

초 록

구조재료에 대한 건전성 평가를 위해서는 가동 환경, 작용 응력, 결함 특성, 기계적 특성 등과 같은 다양한 정보가 필수적이다. 가동 환경과 작용 응력의 경우 설계 정보로부터 대략적인 예측이 가능하고, 결함 특성의 경우 음향 방출 시험 및 초음파 시험으로부터 산업 현장에서 측정이 가능하다. 반면, 재료의 고유한 기계적 특성은 전통적인 파괴적 평가 방법으로 현장에서 측정이 불가능하고, 표준화된 시험 절차에 의해서만 측정이 가능하다. 또한, ASTM (American Society for Testing Materials) 과 같은 재료 시험에 관한 기준은 특정 형상과 크기를 규정하기 때문에, 미세 구조물 혹은 복잡한 형상을 갖는 구조물의 기계적 특성 평가에 큰 어려움이 있다. 따라서, 가동 중 구조물에 대해 건전성 수준을 진단하거나, 복잡·다양해지는 최첨단 산업 제품의 건전성을 평가하기 위해서는 기존 시험법의 한계점을 극복할 수 있는 평가 방법이 필요하다.

기존 경도 측정법으로부터 발전된 연속압입시험법은

기본적으로 경도와 탄성계수를 측정할 수 있을 뿐만 아니라, 하중 및 변위곡선의 탄·소성 해석을 통해 인장물성, 잔류응력, 파괴인성과 같은 고급 물성을 측정할 수 있는 방법이다. 또한, 압입자의 크기 혹은 하중 및 변위 범위를 조절하여 마이크로부터 나노 스케일 하에서 기계적 특성에 대한 측정이 가능하다. 이와 같은 특징과 장점으로 연속압입시험법에 관한 연구가 활발히 이어져 오고 있다. 특히, 다양한 기계적 특성 중 항복강도는 재료의 파손 예측에 가장 기본이 되는 정보이기 때문에, 연속압입시험법과 하중 및 변위곡선을 활용하여 항복강도를 예측하기 위한 많은 연구들이 수행되고 있다.

기존 연구들은 실험적 혹은 해석적 방법을 통해 압입파라미터와 항복강도를 상관시킬 수 있는 모델을 정립하였고, 다양한 가공경화 거동을 갖는 재료에 대하여 제안된 모델의 신뢰성을 검증하였다. 하지만, 기존 연구에 의해 제안된 대부분의 모델은 등방성을 갖는 재료로 가정하여 유도되었기 때문에 “방향성” 에 관한 정보가 배제되었다. 따라서, 냉간/열간 압연과 같은 소성 변형 공정에 의해 제작된

제품과 최근 이슈가 되고 있는 3D 프린팅 재료와 같이 방향성을 나타내는 대상물에 대해서는 적용이 어려울 것으로 예상된다. 또한, 기존 연구들은 연속압입시험에 의해 예측된 항복강도의 정확도에 집중하였을 뿐, 데이터의 변동성과 신뢰성에 대해서는 거의 고려되지 않았다. 특히, 항복강도는 재료의 소성 변형의 시작점이기 때문에 네킹점 에서의 응력보다 변동성이 매우 심하다는 특징을 갖는다. 이러한 데이터의 변동성에 대한 심도 있는 연구가 수행되어야만 시험법의 국제적인 표준화 및 보편화 이루어질 수 있다.

본 연구에서는 방향성이 고려된 항복강도 평가 모델을 유도하기 위해 복잡한 현상을 수학적 방법으로 단순화할 수 있는 차원해석이 도입되었다. 이에 대한 기본적 데이터를 얻기 위해서, 항복강도, 항복강도의 방향비, 가공경화지수를 변경하여 100 가지의 경우에 대한 유한요소해석을 수행하였다. 이를 통해 얻어진 하중 및 변위 데이터를 활용하여 차원해석이 수행되었고, 항복강도의 방향비가 고려된 압입항복강도 평가 모델이 제안되었다. 또한, 압흔 주변에 발생하는 변위 분포를 분석하여

항복강도의 방향비를 평가할 수 있는 모델이 제안되었다. 이는 이미지 분석을 통해 압흔 주변 변위 분포의 해석이 가능한 Digital Image Correlation (DIC) 를 통해 실험적 검증까지 수행되었다. 연속압입시험에 의해 얻어지는 데이터 및 결과의 변동성에 관련해서는 ISO (International Organization for Standardization) 과 같은 국제 표준에 기반하여 불확도 평가 연구가 수행되었다. 불확도 평가를 위한 항복강도 계산 모델은 개선된 Meyer relation 이 사용되었으며, 이에 대해 A형과 B형 불확도가 고려되었다. 최종적으로, 압입 항복강도의 불확도 평가 방법이 제안되었고, 확률 및 통계적 접근을 통해 연속압입시험의 주요 불확도 인자인 시편의 표면 거칠기 및 표면과 압입축 간 각도 기준이 제안되었다.

SCI Papers

1. Seung-Gyu Kim, Najung Kim, Hyung-Seok Shim, **Oh Min Kwon** and Dongil Kwon, Evaluation and Control of Mechanical Degradation of Austenitic Stainless 310S Steel Substrate During Coated Superconductor Processing, *Met. Mater. Int.* (2018)

2. **Oh Min Kwon**, Jongho Won, Jong-hyoung Kim, Changhyun Cho, Eun-chae Jeon and Dongil Kwon, Effects of the Surface Contact on the Uncertainty in Indentation Yield Strength: Surface Roughness and Angular Misalignment, *Met. Mater. Int.* (2019)

3. Jongho Won, Seunggyu Kim, **Oh Min Kwon**, Young-Cheon Kim and Dongil Kwon, Evaluation of tensile yield strength of high-density polyethylene in flat-ended cylindrical indentation: An analytic approach based on the expanding cavity model, *J. Mater. Res.* (2020)

4. **Oh Min Kwon**, Jiyeon Kim, Jinwoo Lee, Jong-hyoung Kim, Hee-Jun Ahn, Ju-Young Kim, Young-Cheon Kim and Dongil Kwon, Compressive Properties of Nanoporous Gold Through Nanoindentation: An Analytical Approach Based on the Expanding Cavity Model, *Met. Mater. Int.* (2020)

5. Changhyun Cho, Seunghun Choi, **Oh Min Kwon**, Seungha Lee, Jong-

hwan Kim and Dongil Kwon, Evaluation of Ballistic Limit Velocity Using Instrumented Indentation Test of 7xxx Aluminum Alloys After Friction Stir Welding, *Met. Mater. Int.* (Published, 2020)

6. Kyeongjae Jeong, Hyukjae Lee, **Oh Min Kwon**, Jinwook Jung, Dongil Kwon and Heung Nam Han, Prediction of uniaxial tensile flow using finite element-based indentation and optimized artificial neural networks, Mater. Des. (Under review, 2020)

Conference Papers

1. Verification of indentation parameters depending on indentation speed based on representative stress and strain approach, *Proc. International Ocean and Polar Engineering Conference* (2016)

2. Structure Assessment Using Instrumented Indentation: Strength, Toughness and Residual Stress, *Proc. International Pipeline Conference* (2018)